

Article

Design, Synthesis and Biological Evaluations of Hydroxypyridone Carboxylic Acids as Inhibitors of HIV Reverse Transcriptase-Associated RNase H

jayakanth kankanala, Karen A. Kirby, Feng Liu, Lena G. Miller, Eva Nagy, Daniel J. Wilson, Michael A Parniak, Stefan G. Sarafianos, and Zhengqiang Wang

J. Med. Chem., **Just Accepted Manuscript** • DOI: 10.1021/acs.jmedchem.6b00465 • Publication Date (Web): 20 Apr 2016

Downloaded from <http://pubs.acs.org> on April 21, 2016

Just Accepted

"Just Accepted" manuscripts have been peer-reviewed and accepted for publication. They are posted online prior to technical editing, formatting for publication and author proofing. The American Chemical Society provides "Just Accepted" as a free service to the research community to expedite the dissemination of scientific material as soon as possible after acceptance. "Just Accepted" manuscripts appear in full in PDF format accompanied by an HTML abstract. "Just Accepted" manuscripts have been fully peer reviewed, but should not be considered the official version of record. They are accessible to all readers and citable by the Digital Object Identifier (DOI®). "Just Accepted" is an optional service offered to authors. Therefore, the "Just Accepted" Web site may not include all articles that will be published in the journal. After a manuscript is technically edited and formatted, it will be removed from the "Just Accepted" Web site and published as an ASAP article. Note that technical editing may introduce minor changes to the manuscript text and/or graphics which could affect content, and all legal disclaimers and ethical guidelines that apply to the journal pertain. ACS cannot be held responsible for errors or consequences arising from the use of information contained in these "Just Accepted" manuscripts.



ACS Publications

1
2
3
4
5
6
7
8
9
10
11
12
13
14
15
16
17
18
19
20
21
22
23
24
25
26
27
28
29
30
31
32
33
34
35
36
37
38
39
40
41
42
43
44
45
46
47
48
49
50
51
52
53
54
55
56
57
58
59
60

Design, Synthesis and Biological Evaluations of Hydroxypyridone Carboxylic Acids as Inhibitors of HIV Reverse Transcriptase-Associated RNase H

*Jayakanth Kankanala^a, Karen A. Kirby^b, Feng Liu^a, Lena Miller^c, Eva Nagy^c, Daniel
J. Wilson^a, Michael A. Parniak^c, Stefan G. Sarafianos^b and Zhengqiang Wang^{*a}*

^a Center for Drug Design, Academic Health Center, University of Minnesota, Minneapolis, MN 55455, USA

^b Department of Molecular Microbiology and Immunology and Department of Biochemistry, University of Missouri School
of Medicine, Christopher S. Bond Life Sciences Center, Columbia, MO 65211, USA

^c Department of Microbiology & Molecular Genetics, University of Pittsburgh School of Medicine, Pittsburgh, PA 15219, USA

Abstract

Targeting the clinically unvalidated reverse transcriptase (RT) associated ribonuclease H (RNase H) for human immunodeficiency virus (HIV) drug discovery generally entails chemotypes capable of chelating two divalent metal ions in the RNase H active site. The hydroxypyridone carboxylic acid scaffold has been implicated in inhibiting homologous HIV integrase (IN) and influenza endonuclease *via* metal chelation. We report herein the

design, synthesis and biological evaluations of a novel variant of the hydroxypyridone carboxylic acid scaffold featuring a crucial *N*-1 benzyl or biarylmethyl moiety. Biochemical studies show that most analogues consistently inhibited HIV RT-associated RNase H in the low micromolar range in the absence of significant inhibition of RT polymerase or IN. One compound showed reasonable cell-based antiviral activity ($EC_{50} = 10 \mu M$). Docking and crystallographic studies corroborate favorable binding to the active site of HIV RNase H, providing a basis for the design of more potent analogues.

1. Introduction

Current HIV antivirals target three of the four virally encoded enzymes (RT polymerase, IN and protease), as well as viral entry proteins and cellular co-receptors.¹ These drugs form the basis for current combination drug therapy of HIV infection (HAART)² by virtue of their distinct mechanisms of action. However, since current HIV therapeutics involve only a few of possible targets, the efficacy of HAART is plagued by the inevitable emergence of HIV mutants resistant to current drugs. Thus, the development of antivirals targeting underexplored and unvalidated processes required for HIV replication may be key to combating current drug-resistant viral strains. One such target is the RT associated RNase H activity.³ RT encodes two distinct enzymatic functions⁴: the polymerase activity that carries out both RNA and DNA dependent DNA polymerization; and the RNase H function that selectively degrades RNA from the RNA/DNA heteroduplex intermediate. The well-known drug families of nucleoside RT inhibitors (NRTIs)⁵ and non-nucleoside RT inhibitors (NNRTIs)⁶ all target the DNA polymerase function of RT; the RNase H function remains a clinically unvalidated target as none of its inhibitors has advanced to

development pipeline.⁷ Nevertheless, the crucial role of RNase H in HIV replication has been well recognized as research showed that active site mutations associated with reduced RNase H biochemical activity conferred attenuated HIV replication in cell culture.⁸ This suggests that potent and selective RNase H inhibition should lead to effective antiviral activity.

The main medicinal chemistry challenge of targeting HIV RNase H is the the lack of appropriate chemical scaffolds supporting specific RNase H inhibition and potent antiviral activity. Reported RNase H inhibitors⁹ generally target the active site by using a chelating triad (Figure 1a; in magenta) for competitive binding to divalent metals, e.g. hydroxyisoquinolinedione (HID, **1**),¹⁰ β -thujaplicinol (**2**),¹¹ and dihydroxycoumarin (**3**).¹² More potent and selective RNase H inhibition was achieved with structurally more elaborate chemotypes, such as diketoacid **4**,¹³ pyrimidinol carboxylic acid **5**,¹⁴ hydroxynaphthyridine **6**¹⁵ and pyridopyrimidone **7**,¹⁶ all featuring a hydrophobic aromatic moiety seemingly important for antiviral activity. Compounds **6–7** are among the very few RNase H inhibitors with reported antiviral activity. Exploiting a chelating core for competitive metal binding is a general medicinal chemistry approach for inhibiting a wide array of enzymes homologous to HIV RNase H.¹⁷ For example, the hydroxypyridone carboxylate core (blue, Figure 1b) for current study has been implicated in influenza endonuclease inhibitor **8**¹⁸ as well as the FDA-approved HIV IN strand transfer inhibitor (INSTI) dolutegravir (DTG)¹⁹ **9** (Figure 1b). Based on the pharmacophore model of RNase H inhibitors **4–7**, chemotype **10** was designed for selectively inhibiting RNase H. We report herein the chemical synthesis, biochemical and antiviral evaluations, molecular modeling, and co-crystal structure of **10**.

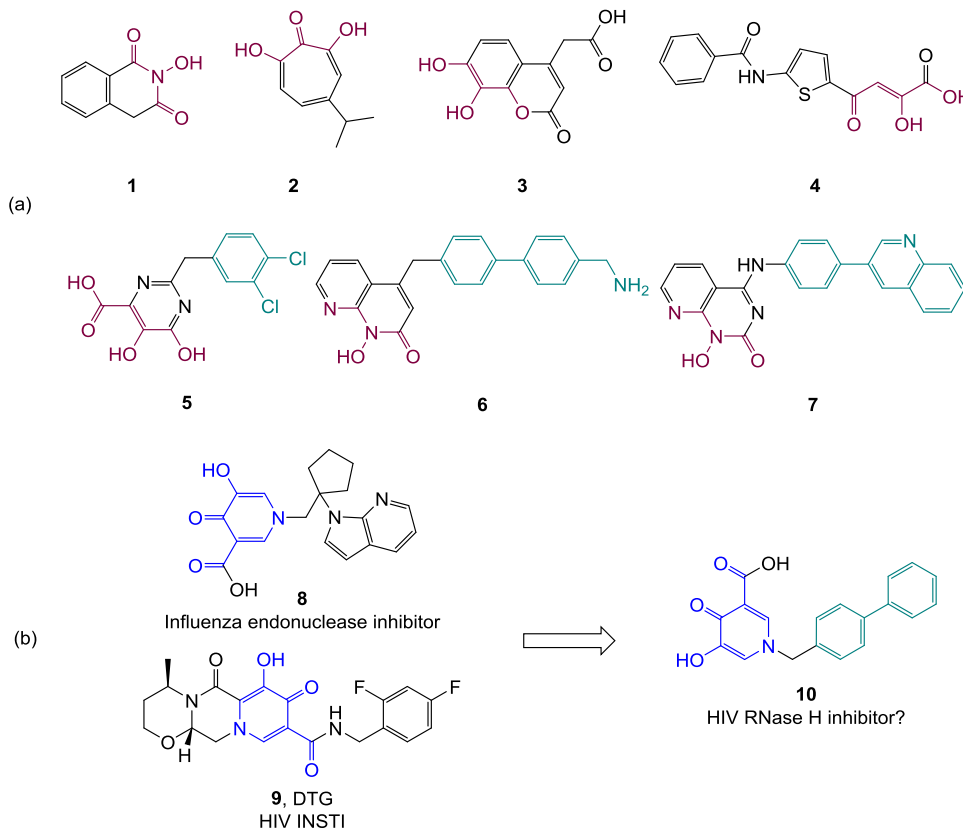


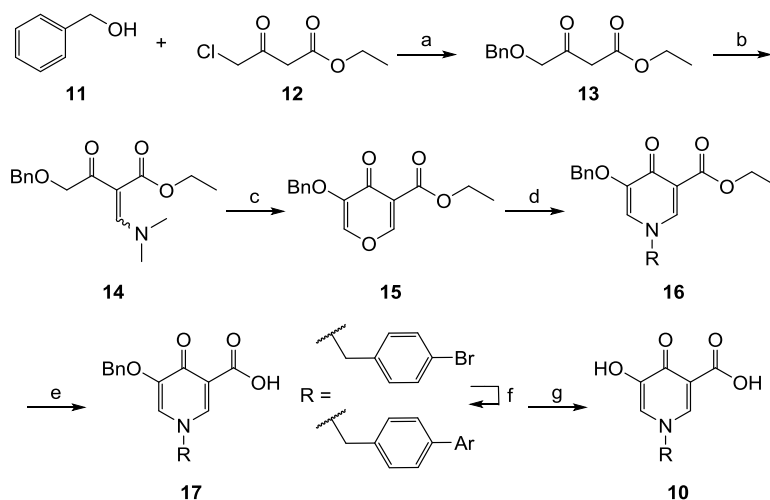
Figure 1. Design of active site RNase H inhibitors. (a) Major chemotypes reported as HIV RNase H active site inhibitors. All chemotypes contain a chelating triad (magenta); scaffolds 4–7 also feature an aryl or biaryl moiety (cyan) connected through a methylene or amino linker; (b) hydroxypyridone carboxylate (blue) is implicated in influenza endonuclease inhibitor 8 and HIV INSTI 9. Active site RNase H inhibitor chemotype 10 based on the same chelating core (blue) is designed. An N-1 aryl or biaryl methyl group is included to mimic scaffolds 5–7.

2. Results and Discussion

Chemistry. The pyridone carboxylate chelating core was constructed using a modification of a previously reported approach.¹⁸ The synthesis began with a benzyl etherification of

the commercially available ethyl chloroacetoacetate (**12**). The resulting ether intermediate (**13**) was subjected to a one-carbon homologation to yield enamine **14**. The subsequent Claisen condensation followed by an immediate cyclization produced the pyrone intermediate **15**. The conversion of the pyrone ring into pyridone (**16**) was effected by heating with an aromatic amine ($R = \text{aryl}$), which upon saponification afforded pyridone carboxylic acid **17**. At this stage, biaryl N-1 substituents were constructed via a Suzuki coupling reaction with a para-bromopenyl substrate (**17**, $R = 4\text{-bromobenzyl}$). The final step of the synthesis involved a debenzoylation to yield the designed analogues (**10a-z**).

Scheme 1^a. Synthesis of hydroxypyridinone carboxylic acids **10a-z**.

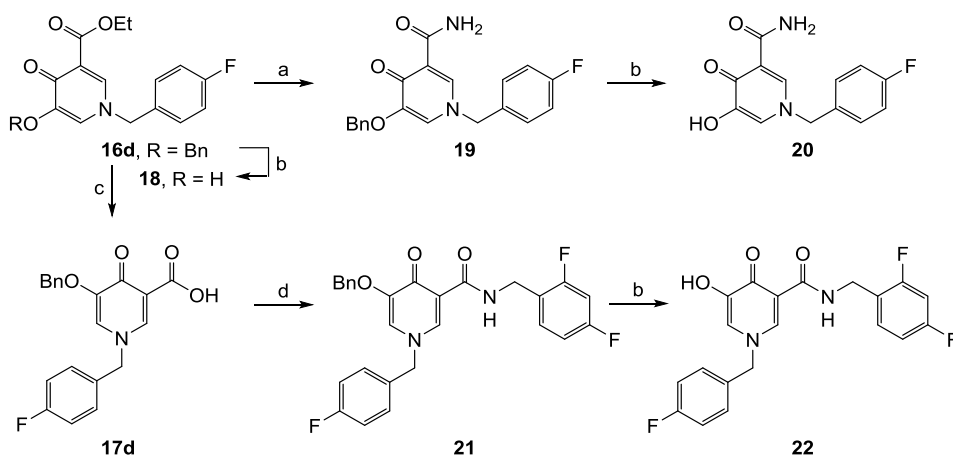


^a Reagents and conditions: a) NaH, THF, r.t, 16 h, 95% ; b) DMF DMA, toluene, r.t, 30%; c) Ethyl formate, KOtBu, THF, r.t, 75%; d) R-NH₂, EtOH, 100 °C, 30-40 min, MW, 40-85%; e) 2N NaOH, EtOH, 90 °C, 4-6 h, 65-95%; f) ArB(OH)₂, K₂CO₃, Pd(PPh₃)₄, DME/H₂O (4:1), 150 °C, 30-40 min, MW, 60-80%; g) TFA, 80 °C, 20 min, MW, 40-87%.

Additional carboxylate derivatives were prepared to provide preliminary structure-activity-relationship (SAR) data (Scheme 2). Direct debenzoylation of pyridone carboxylate **16d**

provided an ester analogue (**18**), and a carboxamide analogue (**20**) was prepared from **16d** via amination and debenzylation. A structurally more elaborate N-benzyl substituted carboxamide (**22**) was synthesized via a three step sequence involving saponification, amide coupling and debenzylation.

Scheme 2^a. Synthesis of hydroxypyridinone carboxylate analogues.



^a Reagents and conditions: a) 7N NH₃/ MeOH, r.t, 48 h, 70%; b) TFA, 80 °C, 20 min, MW, 65—78% c) 2N NaOH, EtOH, 90 °C, 4 h, 87% d) benzyl amine, HATU, DIPEA, DMF, r.t, 12 h, 72%.

Biology: All compounds were evaluated biochemically for inhibition in HIV RT RNase H and polymerase assays. Selected compounds were also tested in an HIV IN strand transfer assay. Antiviral screening was conducted using a HIV-1 single replication cycle assay.

RNase H inhibition: Inhibition of RT-associated RNase H inhibitory activity was evaluated in a biochemical assay²⁰ using three different oligonucleotide duplexes as substrates to probe three distinct modes of RNase H cleavages: HTS-1 for internal cleavages which likely represent the primary mode of RNase H cleavage; HTS-2 for the

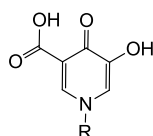
DNA 3' end-directed cleavages allowing specific RNA cuts 17–18 nucleotides downstream from the polymerase active site; and HTS-3 for the RNA 5' end-directed cleavages of recessed RNA templates. Assay results are summarized in Table 1. Most of the hydroxypyridone carboxylate analogues inhibited the internal cleavage (HTS-1) by RNase H in the low- to sub-micromolar range ($IC_{50} = 0.65\text{--}18\text{ }\mu\text{M}$), with some exceptions (**10a–c**, **10n–p**). Secondly, analogues bearing a two-ring (**10r–t**) or a biaryl (**10r–z**) substituent at N-1 position demonstrated significantly more potent inhibition ($IC_{50} = 0.65\text{--}7.7\text{ }\mu\text{M}$) than those with a single-ring substituent (**10b–p**, $IC_{50} = 12\text{--}25\text{ }\mu\text{M}$), with **10q** being the sole exception. N-1 unsubstituted (**10a**) and phenyl substituted (**10b**) analogues were both inactive. These observations strongly corroborate the pharmacophore model that an aryl or biaryl ring separated from the chelating core with a one-atom linker is required for RNase H inhibition and that the biaryl confers better inhibition than the aryl (Fig. 1a, **5–7**). Third the two submicromolar inhibitors, **10x** and **10y**, both have H-bond acceptors and / or donors at the terminus of the biaryl substituent, suggesting interaction of the biaryl with the nucleic acid substrate.

The broadest range of inhibition across all compounds was noted with the HTS-1 substrate, which is not surprising since this substrate was designed to enable highly sensitive detection of inhibitors.²¹ No inhibition was observed using the more rigorous substrates HTS-2 or HTS-3 for analogues with a single ring N-1 substituent (**10b–p**). For analogues with a two-ring N-1 substituent, the same substrate bias was observed with compounds **10r–u** and **10z**, whereas others (**10v–y**) showed nearly equal inhibition with all three substrates.

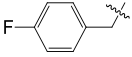
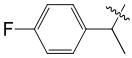
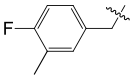
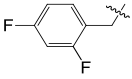
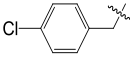
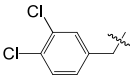
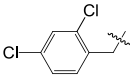
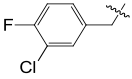
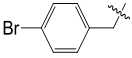
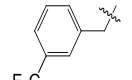
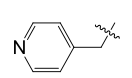
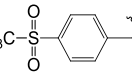
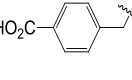
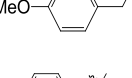
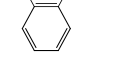
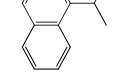
In addition, the biochemical assessment of RNase H inhibition was also carried out with a catalytically active RNase H domain fragment (Table 1, RNase H Fragment). Nearly all analogues inhibited the RNase H fragment in low micromolar range. The data with this fragment confirmed that biaryl substitution confers better inhibition than aryl.

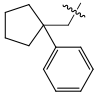
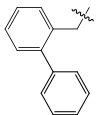
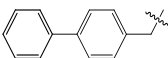
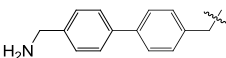
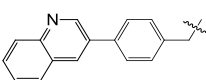
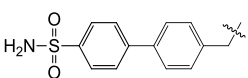
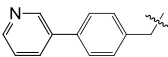
Our SAR analysis was expanded by exploring the importance of the carboxylate functional group by synthesizing analogues of **10d**: the ester **18**, the carboxamide **20** and the 2,4-difluorobenzyl carboxamide **22**. The biochemical assay results showed that esterification abrogated inhibitory activity (compound **18**), whereas the inhibitory activity was preserved with carboxamide modification (**20** and **22**). Importantly, the 2,4-difluorobenzyl carboxamide **22** provided significantly better inhibition of RT polymerase and RNase H activities compared to the parent carboxylic acid **10d**. This same modification may also provide integrase inhibition, leading to multi-target efficacy in a single compound.

Table 1. Biochemical assay results of *N* substituted pyridone-carboxylic acid analogues (**10**) against HIV RT



Compd	R	RNH IC ₅₀ ^a (μM)			RNH Fragment ^e IC ₅₀ (μM)	RT Pol IC ₅₀ ^a (μM)
		HTS-1 ^b	HTS-2 ^c	HTS-3 ^d		
10a	H	>25	>25	>25	22 ± 2.3	>25
10b		>25	>25	>25	>25	>25
10c		>25	>25	>25	11 ± 1.5	>25

10d		17	>25	>25	7.8 ± 0.6	>25
10e		16 ± 4.5	>25	>25	5.3 ± 0.5	>25
10f		17 ± 5.2	>25	>25	9.8 ± 0.7	>25
10g		13 ± 2.1	>25	>25	6.8 ± 0.9	>25
10h		17	>25	>25	7.8 ± 0.8	>25
10i		14	>25	>25	4.7 ± 0.5	>25
10j		12	>25	>25	4.2 ± 0.4	>25
10k		18 ± 2.8	>25	>25	9.8 ± 0.5	>25
10l		>25	>25	>25	>25	>25
10m		18 ± 4.5	>25	>25	11 ± 1.9	>25
10n		>25	>25	>25	>25	>25
10o		>25	>25	>25	25 ± 2.0	>25
10p		>25	>25	>25	14 ± 1.1	>25
10q		2.5 ± 0.2	15 ± 0.5	20 ± 2.2	4.8 ± 0.2	>25
10r		2.7 ± 0.6	4.3 ± 0.4	5.4 ± 1.1	1.9 ± 0.1	8.5 ± 1.5
10s		7.0 ± 0.7	>25	13 ± 2.7	3.7 ± 0.6	19 ± 5.5

10t		1.5 ± 0.2	5.1 ± 0.5	4.9 ± 2.2	8.2 ± 0.1	1.8 ± 0.1
10u		7.7 ± 2.4	25 ± 1.5	>25	5.1 ± 0.3	>25
10v		2.5 ± 0.4	2.8 ± 0.6	2.9 ± 0.3	1.8 ± 0.3	2.2 ± 0.1
10w		3.2 ± 0.3	4.4 ± 0.6	3.9 ± 0.4	4.4 ± 0.5	3.2 ± 0.8
10x		0.90 ± 0.05	1.2 ± 0.1	0.90 ± 0.2	1.0 ± 0.01	1.1 ± 0.1
10y		0.65 ± 0.05	1.5 ± 0.2	1.0 ± 0.2	1.3 ± 0.05	1.2 ± 0.1
10z		3.6 ± 0.2	10 ± 0.6	15 ± 6.2	2.6 ± 0.6	>25
18	--	>25	>25	>25	>25	>25
20	--	12 ± 1.8	>25	>25	6.8 ± 0.7	>25
22	--	7.5 ± 0.4	4.5 ± 0.8	4.9 ± 1.0	3.2 ± 0.2	2.4 ± 0.1

^a IC₅₀: concentration of a compound producing 50% inhibition, expressed as mean \pm standard deviation from at least three independent experiments.

^b Substrate that measures internal cleavage.

^c Substrate that measures DNA 3' end directed cleavage.

^d Substrate that measures RNA 5' end directed cleavage.

^e Reconstituted HIV RNase H domain.

Polymerase inhibition: All compounds were evaluated for inhibition of RT RNA-dependent DNA polymerase activity. A sharp SAR trend was noted in which the N-1 unsubstituted analogue **10a** and all one-ring substituted analogues (**10b–q**) showed no

inhibitory activity (at concentrations up to 25 μ M) whereas most two-ring substituted analogues (**10r–t** and **10v–y**) inhibited RT pol with potencies nearly equal to RNase H inhibition. Although the mechanism of this polymerase inhibition remains unclear, we speculate that these inhibitors may block the polymerase active site metal-binding triad to prevent facile catalysis of nucleotide incorporation.

Order-of-addition RNase H inhibition assays: To determine whether lead analogues retain inhibitory activity when added after the RNA/DNA substrate we performed order-of-addition assays to examine the effect of various pre-incubation conditions on RT-associated RNase H inhibition. We tested six of the most potent inhibitors of RT-associated RNase H using β -thujaplicinol for comparison under conditions similar to those run for the *in vitro* RNase H inhibition assays in which the RNA/DNA substrate is in excess of the RT (Table 1). Generally, the inhibitors are most potent against RNase H activity when they are added to RT before the RNA/DNA substrate (Table 2). When the RT/substrate complex is formed before addition of compound, the inhibitor potency is decreased in all cases, including the previously published β -thujaplicinol.²² Under these conditions, analogue **10x** is the most potent of the inhibitors against cleavage of the pre-formed RT/substrate complex (>50% inhibition), suggesting it can compete with the substrate for binding to RT.

When these assays were carried out using RT in excess of the RNA/DNA substrate, which more closely resembles actual conditions in the virion, generally the analogues more efficiently maintain effective inhibition against the pre-formed RT/substrate complex. Under conditions of excess RT compared to RNA/DNA substrate, **10y** is the most potent inhibitor of the RT/substrate complex, as it blocks 80% of the RT-associated RNase H activity (Table 3).

Table 2. Order-of-addition RNase H inhibition assay results

% Inhibition				
1. Pre-Incubation (10 min at 37 °C)	RT + Inhibitor	RT + MgCl ₂ + Inhibitor	RT + Inhibitor + HTS-1	RT + HTS-1
2. Reaction Initiation (10 min at 37 °C)	HTS-1 + MgCl ₂	HTS-1	MgCl ₂	Inhibitor + MgCl ₂
10q^a	69% ± 5% ^b	52% ± 17%	27% ± 4%	21% ± 13%
10r	58% ± 0%	51% ± 7%	35% ± 3%	28% ± 5%
10t	75% ± 5%	84% ± 1%	38% ± 2%	18% ± 13%
10v	68% ± 9%	36% ± 12%	37% ± 7%	21% ± 19%
10x	95% ± 1%	68% ± 10%	66% ± 8%	50% ± 7%
10y	97% ± 1%	79% ± 9%	68% ± 6%	14% ± 3%
β-thujaplicinol	100% ± 1%	99% ± 1%	79% ± 8%	12% ± 4%

^aFinal reaction conditions: 100 nM HIV RT, 250 nM HTS-1, 6 mM MgCl₂, 30 μM inhibitor.

^bValues are reported as mean ± standard deviation from two independent experiments.

Table 3. Order-of-addition RNase H inhibition assay results in the presence of excess RT

% Inhibition		
1. Pre-Incubation (10 min at 37 °C)	RT + Inhibitor	RT + HTS-1
2. Reaction Initiation	HTS-1 + MgCl ₂	Inhibitor + MgCl ₂

(2 min at 37 °C)

10q^a	70% ± 9% ^b	58% ± 3%
10r	82% ± 1%	61% ± 8%
10t	42% ± 1%	15% ± 5%
10v	78% ± 2%	59% ± 6%
10x	91% ± 0%	74% ± 4%
10y	92% ± 1%	80% ± 1%
β-thujaplicinol	100% ± 0%	98% ± 4%

^aFinal reaction conditions: 300 nM HIV RT, 50 nM HTS-1, 0.5 mM EDTA, 6 mM MgCl₂, 30 μM inhibitor.

^bValues are reported as mean ± standard deviation from two independent experiments.

Table 4. Comparison of biochemical inhibition against RT RNase H, RT pol and INST

<i>Compd</i>	<i>RT RNase H IC₅₀^a(μM)</i>	<i>RT Pol IC₅₀(μM)</i>	<i>IN IC₅₀(μM)</i>
10a	>25	>25	>100
10b	>25	>25	37
10c	>25	>25	35
10d	17	>25	35
10e	16 ± 4.5	>25	34
10f	17 ± 5.2	>25	>100

10g	13 ± 2.1	>25	>100
10h	17	>25	67
10i	14	>25	36
10j	12	>25	25
10k	18 ± 2.8	>25	44.5 ± 18.1
10l	>25	>25	>100
10m	18 ± 4.5	>25	>100
10n	>25	>25	>100
10o	>25	>25	>100
10p	>25	>25	>100
10q	2.5 ± 0.2	>25	>100
10r	2.7 ± 0.6	8.5 ± 1.5	23
10s	7.0 ± 0.7	19 ± 5.5	2.26 ± 0.87
10t	1.5 ± 0.2	1.8 ± 0.1	14
10u	7.7 ± 2.4	>25	17
10v	2.5 ± 0.4	2.2 ± 0.1	22
10w	3.2 ± 0.3	3.2 ± 0.8	7.79 ± 1.93
10x	0.90 ± 0.05	1.1 ± 0.1	16.0 ± 6.5
10y	0.65 ± 0.05	1.2 ± 0.1	>100
10z	3.6 ± 0.2	>25	35.0 ± 10.0
18	>25	>25	>100
20	12 ± 1.8	>25	32
22	7.5 ± 0.4	2.4 ± 0.1	>100

^a Data with HTS-1 as substrate

HIV integrase strand transfer inhibition: HIV IN and RNase H share similar active site configurations, thus inhibitors of these enzymatic functions entail overlapping pharmacophore features. Selective inhibition of RNase H over INST is therefore particularly important in RNase H inhibitor discovery. To assess the selectivity profile of the new pyridone chemotype, all analogues were tested for INST activity (Table 4).

While most of the compounds showed some INST inhibitory activity, this inhibitory activity was much weaker ($14\ \mu\text{M}$ - $> 100\ \mu\text{M}$) than that provided against RT RNase H, suggesting that the hydroxypyridone carboxylate core represents an interesting chemotype for future development of specific inhibitors of HIV RNase H.

Antiviral assay: All compounds were screened in a previously reported single replication cycle antiviral assay²³ to gauge their ability in inhibiting HIV replication in cell culture. Although most compounds did not inhibit HIV-1 replication in this assay, analogue **10r** inhibited HIV-1 replication in a dose-dependent manner (Figure 2, $\text{EC}_{50} = 10\ \mu\text{M}$) without cytotoxicity at concentrations up to $25\ \mu\text{M}$ ($\text{CC}_{50} > 25\ \mu\text{M}$). This is an important and exciting observation as very few RNase H inhibitors to date have been reported to possess antiviral activity in cell-based assays.

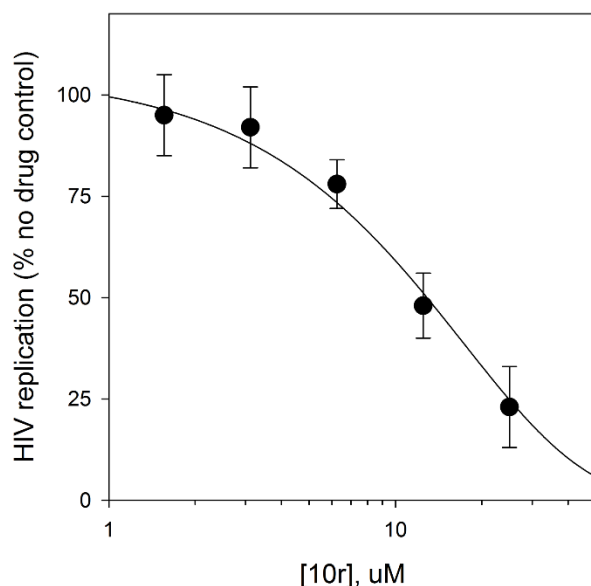


Figure 2. Dose response antiviral effect of **10r** against HIV-1. Experiments were done in triplicate with each data point. The antiviral EC_{50} is calculated to be 10 μ M.

Molecular modeling: Docking analysis was performed with Glide XP(v.6.4)²⁴⁻²⁵ using two metal sites as a constraint. The predicted binding mode of compound **10r** in the active site of RNase H suggests an interaction between the 4-oxo-1,4-dihydropyridine carboxylic acid core (chelating triad) and the two active site metal cations (coordinated to essential active site residues D443, E478, D498 and D549). The hydroxyl group at 5-position of **10r** can form H-bonding interactions with H539 which would stabilize inhibitor positioning near the active site metal-chelating residues D443, E478, D498 and D549, all of which are crucial for RT-RNase H activity. The flexible methylene linker at N1 position of the pyridone core induces a conformational flexibility in the inhibitor that allows π -stacking interaction between the naphthalene ring of the ligand and RNase H residues H539 and A538 and L560. This interaction may limit the conformational flexibility of the loop with

H539 and thus impact on efficiency of RNase H catalytic activity. Notably, a similar binding mode was observed for RT complexes with dsDNA or RNA-DNA hybrids as reported by Harrison et.al.²⁶ and Sarafianos et.al.²⁷ The predicted binding mode of **10r** is shown in Figure 3a within the active site of RNase H. Compound **10y** was predicted to bind in an identical fashion to that of **10r**. Compounds **10r** and **10y** were observed to overlay with the pyrimidinol carboxylic acid core (**5**) and mimic the interactions within the RNaseH to a greater extent as depicted in Figure 3b and 3c.

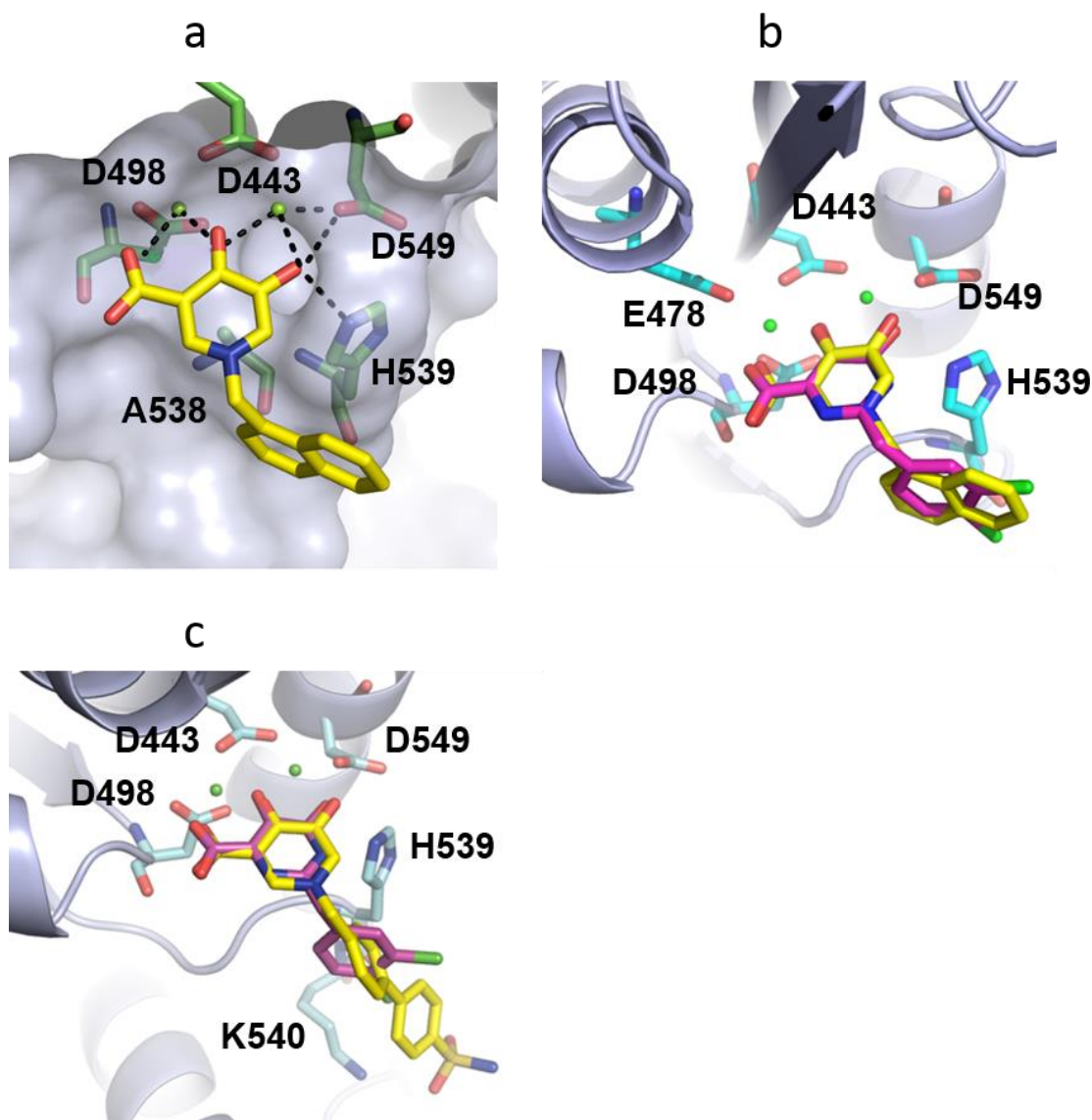


Figure 3. Molecular modeling of analogues **10r** and **10y** at the RNase H active site and comparison to crystal structure of the HIV RNase H domain in complex with pyrimidinol carboxylic acid. a) Predicted binding mode of **10r** within active site of RNase H (PDB code: 3HYF). Active site residues are highlighted in green sticks with metal ions as spheres. Some chelating and H-bond interactions are depicted as black dotted lines. b) Overlay of **10r** (yellow) on the crystal structure of RNase H with pyrimidinol carboxylic acid (magenta). c) Overlay of **10y** (yellow) on the crystal structure of RNase H with pyrimidinol carboxylic acid (magenta).

Crystal structure of HIV RT in complex with 10y: In order to further understand the molecular details of HIV RT-associated RNase H inhibition by hydroxypyridone carboxylate analogues, we solved the crystal structure of HIV RT in complex with the most potent RNase H inhibitor from the *in vitro* assays, **10y**, at 2.9 Å resolution. The asymmetric unit comprises two RT molecules, and therefore two distinct RNase H active sites. Analogue **10y** is only observed at one RT active site in the asymmetric unit, most likely due to partial occlusion of one RNase H active site by the fingers subdomain of the second RT molecule. Unlike other RT/RNase H active site-directed inhibitor complex structures,²⁸⁻²⁹ the RT/**10y** complex was crystallized without a non-nucleoside RT inhibitor (NNRTI), leaving the positions of the two p66 Thumb domains in a closed conformation, similar to other reported unliganded RT structures.³⁰⁻³⁴

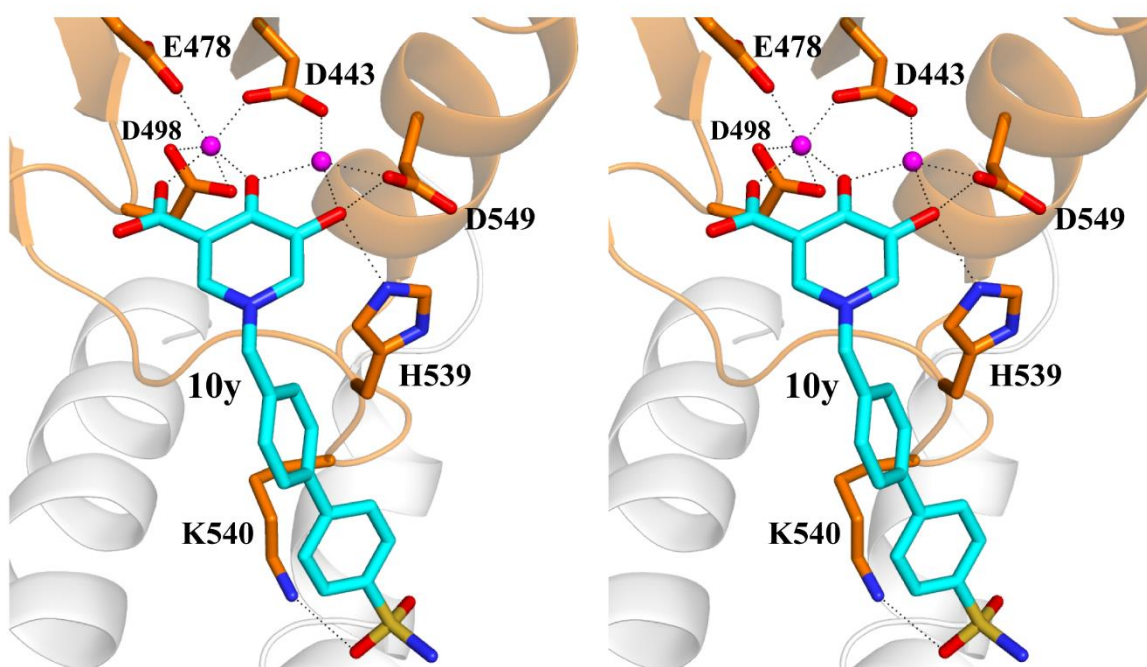


Figure 4. X-ray crystal structure of HIV RT in complex with analogue **10y**. Cross-eyed stereo view of **10y** (cyan) bound at the RNase H active site of HIV RT. The RNase H domain of RT is shown in orange, the p51 in light gray. Conserved active site residues are shown as sticks, and Mg^{2+} ions are shown as magenta spheres. Chelating and H-bond interactions are indicated by dashed lines. Cartoon was prepared by PyMOL³⁵ and crystallographic coordinates have been submitted to the Protein Data Bank (PDB ID: 5J1E).

In the occupied RNase H active site, two Mg^{2+} ions are bound by conserved active site residues D443, E478, D498, and D549. Analogue **10y** chelates both Mg^{2+} ions through the carboxylate, carbonyl, and hydroxyl groups of the pyrimidone (Figure 4), in a manner similar to that of a previously reported RT/pyrimidinol carboxylic acid inhibitor.²⁹ **10y** interacts directly with RT through interactions between the hydroxyl group of the pyridone

and H539, and the sulfonamide group of the N-1 substituted biaryl moiety with K540 (Figure 4). These additional interactions with the RT enzyme likely provide increased stability to the RT/**10y** complex and may potentially explain the potent RNase H inhibition observed for **10y** in the *in vitro* assays (Table 1).

Compared to other analogues, **10y** was found to be the most potent inhibitor of RT-associated RNase H inhibition. Structural insights suggest that the length provided by the N-1 substituted biaryl moiety could be important for RNase H inhibition, since many of the shorter phenyl-substituted analogues (**10b-q**) were less potent. It also appears that charge may also contribute to potent inhibition, as other biaryl-substituted compounds without charged groups (such as **10w**) were less effective inhibitors of RNase H activity. Furthermore, *para* substitution of the biaryl moiety relative to the pyridone ring seems to position the biaryl group in a favorable position to have potential interactions with RT, which may not be achievable with *ortho*-substituted analogues such as **10u** and may explain this analogue's decreased potency.

Conclusions

New hydroxypyridone carboxylate analogues featuring an N-1 benzyl or biarylmethyl moiety were designed and synthesized as potential inhibitors of HIV RT associated RNase H. *In vitro* biochemical assays showed that analogues with a two-ring substituent at N-1 are significantly more potent than those with a one-ring substituent against all three modes of RNase H cuts as well as the RT polymerase function. While some analogues also inhibited strand transfer activity of HIV IN, this inhibition was substantially less than that for RT RNase H inhibition, suggesting that the pyridone chemotype may represent an

interesting scaffold for development of RNase H-specific inhibitors. Importantly, compound **10r** exhibited significant inhibitory activity in a cell-based antiviral assay with an EC₅₀ of 10 μ M. Molecular docking of **10r** and the crystal structure of RT/**10y** corroborate for hydroxypyridone carboxylate analogues a mechanism of active site binding for RNase H inhibition. The mechanism of the observed polymerase inhibition remains unclear. These results indicate that the hydroxypyridone carboxylate chemotype previously implicated in the inhibition of INST and influenza endonuclease can be valuable in the discovery of HIV antivirals targeting the RT-associated RNase H.

Experimental

Chemistry: General Procedures. All commercial chemicals were used as supplied unless otherwise indicated. Flash chromatography was performed on a Teledyne Combiflash RF-200 with RediSep columns (silica) and indicated mobile phase. All moisture sensitive reactions were performed under an inert atmosphere of ultra-pure argon with oven-dried glassware. ¹H and ¹³C NMR spectra were recorded on a Varian 600 MHz spectrometer. Mass data were acquired on an Agilent TOF II TOS/MS spectrometer capable of ESI and APCI ion sources. Analysis of sample purity was performed on a Varian Prepstar SD-1 HPLC system with a Phenomenex Gemini, 5 micron C18 column (250mm x 4.6 mm). HPLC conditions: solvent A = H₂O, solvent B = MeCN; flow rate = 1.0 mL/min; compounds were eluted with a gradient of 5% MeCN/H₂O for 0-5 min and to 95% MeCN/H₂O from 5-30 min followed by 100% MeCN from 35-40 min. Purity was determined by total absorbance at 254 nm. All tested compounds have a purity \geq 98%.

Ethyl-4-(benzyloxy)-3-oxobutanoate (13). To a suspension of 60% NaH (66.83 mmol, 2.2 eq) in THF (20 mL) at 0 °C was added benzyl alcohol (30.37 mmol, 1.05 eq) and the resulting mixture was stirred at r.t for 2h. To this mixture was then added ethyl-4-chloroacetoacetate (30.37 mmol, 1.0 eq) dropwise over 30 min and the resulting clear yellow solution was stirred at r.t overnight before it was cooled to 5 °C, acidified to pH = 4 using 5% HCl and extracted with the EtOAc (2 x 25 mL). The combined organics were washed with brine, dried over Na₂SO₄ and concentrated *in vacuo* to yield the desired product (**13**) as orange oil. The crude material was used for next step without further purification. Yield: 95% (6.8 g). ¹H NMR (600 MHz, CDCl₃) δ 7.40-7.28 (m, 5H), 4.59 (s, 2H), 4.18 (q, *J* = 7.1 Hz, 2H), 4.14 (s, 2H), 3.54 (s, 2H), 1.25 (t, *J* = 7.1 Hz, 3H).

4-Benzyloxy-2-(1-dimethylaminomethylidene)-3-oxo-butyric acid ethyl ester (14). To a solution of **13** (28.36 mmol, 1.0 eq) in toluene (30 mL) was added DMF DMA (42.54 mmol, 1.5 eq) and the resulting mixture was stirred at r.t for 12 h. The reaction mixture was quenched by adding water and was acidified (pH = 4) using 5% HCl. The aqueous solution was extracted using EtOAc (2 x 20 mL). The combined organics were washed with NaHCO₃, and brine, dried over Na₂SO₄ and concentrated *in vacuo*. The crude mixture was purified using CombiFlash with eluent starting from hexane/EtOAc (4:1) to hexane/EtOAc (1:1) to yield the desired product (**14**) as yellow oil. Yield: 30% (2.45 g); ¹H NMR (600 MHz, DMSO-d₆) δ 7.67 (s, 1H), 7.38-7.30 (m, 4H), 7.28 (t, *J* = 6.8 Hz, 1H), 4.45 (s, 2H), 4.30 (s, 2H), 4.06 (q, *J* = 7.1 Hz, 2H), 3.24 (brs, 3H), 2.73 (brs, 3H), 1.17 (t, *J* = 7.1 Hz, 3H).

General method for the synthesis of pyrone: Ethyl-5-(benzyloxy)-4-oxo-4H-pyran-3-carboxylate (15). To a suspension of potassium tert-butoxide (1M in THF; 15.79 mmol,

2.0 eq) in THF (14 mL) was added ethyl formate (33.8 mmol, 4.3 eq) and the mixture was stirred at r.t for 30 min before compound **13** (7.89 mmol, 1.0 eq) in THF (14 mL) was added dropwise over 10 min. The resulting mixture was stirred at r.t for 8 h and quenched by adding 2N HCl (12 mL). After extraction with the EtOAc (2 x 20 mL), the combined organics were washed with NaHCO₃ (2 x 10 mL), water (30 mL), brine (30 mL), dried over Na₂SO₄ and concentrated *in vacuo* to leave brownish yellow oil. This crude product was triturated by adding hexanes to yield the desired product (**15**) as brown solid. Yield: 75% (1.62 g); ¹H NMR (600 MHz, DMSO-d₆) δ 8.72 (d, *J* = 0.8 Hz, 1H), 8.30 (d, *J* = 0.8 Hz, 1H), 7.49-7.33 (m, 5H), 4.95 (s, 2H), 4.22 (q, *J* = 7.1 Hz, 2H), 1.25 (t, *J* = 7.1, 3H).

General method for the synthesis of 4-oxo-dihydropyridine esters (16a-16s). To a solution of **15** (1.0 eq) in EtOH (5 mL) was added amine (2.0 eq) and the resulting mixture was heated at 100 °C for 40 min under microwave conditions. After the solvent was removed *in vacuo* the residue was purified using CombiFlash to produce the crude product as colorless oil which was triturated with hexanes/EtOAc to yield the titled compound as colorless solid (**16a-16s**).

Ethyl-1-benzhydryl-5-(benzyloxy)-4-oxo-1,4-dihydropyridine-3-carboxylate (16a).

¹H NMR (600 MHz, DMSO-d₆) δ 8.18 (d, *J* = 1.8 Hz, 1H), 7.48 – 7.40 (m, 6H), 7.36 – 7.31 (m, 3H), 7.29-7.26 (m, 3H), 7.11 (d, *J* = 7.0 Hz, 4H), 6.92 (s, 1H), 4.93 (s, 2H), 4.14 (q, *J* = 7.1 Hz, 2H), 1.19 (t, *J* = 7.1 Hz, 3H).

General procedure for saponification: (17a-17s). To a solution of **16** (1.0 eq) in EtOH (5 mL) was added 2N NaOH (10 mL). The resulting mixture was heated at 90 °C for 6 h and was then cooled to r.t and concentrated *in vacuo*. The resulting solution was acidified

(pH = 3) using 2N HCl. The precipitate was collected *via* filtration, washed with water, and then dried to obtain the titled compound as colorless solid (**17**).

1-Benzhydryl-5-(benzyloxy)-4-oxo-1, 4-dihydropyridine-3-carboxylic acid (17a). ¹H NMR (600 MHz, CD₃OD) δ 8.41 (s, 1H), 7.48 (s, 1H), 7.42-7.39 (m, 6H), 7.27-7.26 (m, 5H), 7.06 (d, *J* = 3.9 Hz, 4H), 6.92 (s, 1H), 5.05 (s, 2H).

General procedure for Suzuki coupling (17w-17z). The mixture of **17l** (1.0 eq), boronic acid (1.6 eq), Pd (PPh₃)₄ (0.065 eq), K₂CO₃ (3.6 eq) in DME/H₂O (4:1) was irradiated at 150 °C for 30 min under microwave conditions. The black residue formed was filtered through celite and the solvent was concentrated *in vacuo*. The resulting aqueous solution was acidified (pH = 3) using 2N HCl. A white precipitate was obtained *via* filtration, washed with water and dried under vacuum to furnish the desired compound as colorless solid (**17w-17z**).

1-((4'-(Aminomethyl)-[1,1'-biphenyl]-4-yl)methyl)-5-(benzyloxy)-4-oxo-1,4-dihydropyridine-3-carboxylic acid (17w). ¹H NMR (600 MHz, DMSO-d₆): δ 8.79 (s, 1H), 8.18 (s, 1H), 7.67 (d, *J* = 7.8 Hz, 2H), 7.75 – 7.60 (m, 4H), 7.52 – 7.35 (m, 4H), 7.35 – 7.17 (m, 5H), 5.41 (s, 2H), 5.11 (s, 2H), 4.08 (s, 2H).

5-(Benzyloxy)-1-(4-fluorobenzyl)-4-oxo-1,4-dihydropyridine-3-carboxamide (19). To a solution of **16d** (90 mg) in methanol was added NH₃ in MeOH (7N, 4 mL) and the resulting solution was stirred at r.t for 48 h. A white precipitate was collected *via* filtration, washed with methanol, and then dried under high vacuum to yield the carboxamide as colorless solid (**19**). Yield: 70%. ¹H NMR (600 MHz, DMSO-d₆): δ 9.47 (s, 1H), 8.52 (s,

3H), 7.81 (s, 1H), 7.44 (s, 1H), 7.35 (m, 7H), 7.24 – 7.15 (m, 2H), 5.22 (s, 2H), 5.00 (s, 2H).

General procedure for amide coupling: 5-(benzyloxy)-N-(2, 4-difluorobenzyl)-1-(4-fluorobenzyl)-4-oxo-1, 4-dihydropyridine-3-carboxamide (21). To a mixture of **17d** (1.0 eq) in DMF (5 mL) was added HATU (1.2 eq), DIPEA (1.2 eq), amine (1.2 eq) and the resulting reaction mixture was stirred at r.t for 12 h. The reaction was quenched with water and extracted with the EtOAc (2 x20 mL). The combined organics were washed with 1N HCl (2 x 10 mL), NaHCO₃ (2 x 10 mL), water (30 mL), brine (30 mL) and dried over Na₂SO₄. The solvent was removed *in vacuo* to produce the crude product as yellow solid which was purified using CombiFlash with 0-100% EtOAc as an eluent to furnish the titled compound as colorless solid (**21**). Yield: 72%. ¹H NMR (600 MHz, DMSO-d₆) δ 10.61 (t, *J* = 5.8 Hz, 1H), 8.57 (d, *J* = 1.7 Hz, 1H), 7.87 (d, *J* = 1.7 Hz, 1H), 7.37 (m, 7H,), 7.22 (m, 4H), 7.05 (dd, *J* = 8.4, 6.4 Hz, 1H), 5.26 (s, 2H), 5.02 (s, 2H), 4.51 (d, *J* = 5.8 Hz, 2H).

General procedure for *O*-debenzylation: (10a-10z, 18, 20, 22). A mixture of **17** (1.0 eq) in TFA (2 mL) was irradiated at 80 °C for 20 min under microwave conditions. The solvent was removed *in vacuo* to produce the crude product as pale yellow solid which was triturated in methanol and ether to produce the titled compound as colorless solid (**10a-10z, 18, 20, 22**).

5-Hydroxy-4-oxo-1, 4-dihydropyridine-3-carboxylic acid (10a). ¹H NMR (600 MHz, DMSO-d₆): δ 12.74 (s, 1H), 9.84 (s, 1H), 8.31 (s, 1H), 7.69 (s, 1H). ¹³C NMR (150 MHz, DMSO-d₆) δ 171.8, 166.6, 148.1, 137.0, 122.4, 113.3. HRMS-ESI (–) *m/z* calculated for C₆H₄NO₄ 154.0146 [M-H][–], found: 154.0148.

5-Hydroxy-4-oxo-1-phenyl-1,4-dihydropyridine-3-carboxylic acid (10b). ^1H NMR (600 MHz, DMSO- d_6): 10.22 (s, 1H), 8.46 (d, $J = 2.3$ Hz, 1H), 8.05 (d, $J = 2.3$ Hz, 1H), 7.74-7.68 (m, 2H), 7.63-7.52 (m, 3H). ^{13}C NMR (150 MHz, DMSO- d_6) δ 171.8, 166.0, 148.8, 142.9, 139.6, 130.3, 129.6, 125.8, 123.9, 113.8. HRMS-ESI (–) m/z calculated for $\text{C}_{12}\text{H}_8\text{NO}_4$ 230.0459 $[\text{M}-\text{H}]^-$, found: 230.0468.

1-Benzyl-5-hydroxy-4-oxo-1,4-dihydropyridine-3-carboxylic acid (10c). ^1H NMR (600 MHz, DMSO- d_6): δ 10.06 (s, 1H), 8.67 (d, $J = 2.0$ Hz, 1H), 7.83 (d, $J = 2.0$ Hz, 1H), 7.51 – 7.31 (m, 5H), 5.35 (s, 2H). ^{13}C NMR (150 MHz, DMSO- d_6) δ 170.8, 165.0, 148.3, 139.9, 135.4, 128.8, 128.4, 127.9, 125.5, 113.0, 59.8. HRMS-ESI (–) m/z calculated for $\text{C}_{13}\text{H}_{10}\text{NO}_4$ 244.0615 $[\text{M}-\text{H}]^-$, found: 244.0627.

1-(4-Fluorobenzyl)-5-hydroxy-4-oxo-1,4-dihydropyridine-3-carboxylic acid (10d). ^1H NMR (600 MHz, DMSO- d_6): 10.06 (s, 1H), 8.68 (d, $J = 2.0$ Hz, 1H), 7.84 (d, $J = 2.0$ Hz, 1H), 7.51 (dd, $J = 8.5, 5.5$ Hz, 2H), 7.45 (t, $J = 8.8$ Hz, 2H), 5.33 (s, 2H). ^{13}C NMR (150 MHz, DMSO- d_6) δ 171.3, 166.3, 148.9, 140.6, 132.2, 130.7, 116.5, 115.8, 115.6, 113.5, 59.5. HRMS-ESI (–) m/z calculated for $\text{C}_{13}\text{H}_9\text{FNO}_4$ 262.0521 $[\text{M}-\text{H}]^-$, found: 262.0531.

1-(1-(4-Fluorophenyl) ethyl)-5-hydroxy-4-oxo-1,4-dihydropyridine-3-carboxylic acid (10e). ^1H NMR (600 MHz, DMSO- d_6): δ 10.05 (s, 1H), 8.64 (d, $J = 2.2$ Hz, 1H), 7.83 (d, $J = 2.2$ Hz, 1H), 7.61 – 7.51 (m, 2H), 7.35 – 7.08 (m, 2H), 5.78 (q, $J = 7.1$ Hz, 1H), 1.86 (d, $J = 7.1$ Hz, 3H). ^{13}C NMR (150 MHz, DMSO- d_6) δ 171.1, 166.1, 163.0, 148.9, 138.9, 135.3, 129.5, 123.6, 116.1, 113.3, 64.9, 19.3. HRMS-ESI (–) m/z calculated for $\text{C}_{14}\text{H}_{11}\text{FNO}_4$ 276.0678 $[\text{M}-\text{H}]^-$, found: 276.0682.

1-(4-Fluoro-3-methylbenzyl)-5-hydroxy-4-oxo-1,4-dihydropyridine-3-carboxylic acid (10f). ^1H NMR (600 MHz, DMSO- d_6): δ 10.06 (s, 1H), 8.66 (d, $J = 2.1$ Hz, 1H), 7.82 (d,

$J = 2.1$ Hz, 1H), 7.39 (dd, $J = 7.2, 1.6$ Hz, 1H), 7.34 (m, 1H), 7.21 (m, 1H), 5.29 (s, 2H).

^{13}C NMR (150 MHz, DMSO- d_6) δ 171.1, 166.2, 161.8, 160.2, 148.7, 140.2, 131.9, 131.6, 128.2, 127.9, 125.2, 113.3, 59.5, 14.2. HRMS-ESI (–) m/z calculated for $\text{C}_{14}\text{H}_{11}\text{FNO}_4$ 276.0678 $[\text{M}-\text{H}]^-$, found: 276.0687.

1-(2,4-Difluorobenzyl)-5-hydroxy-4-oxo-1,4-dihydropyridine-3-carboxylic acid (10g).

^1H NMR (600 MHz, DMSO- d_6): δ 10.11 (s, 1H), 8.60 (d, $J = 1.7$ Hz, 1H), 7.76 (d, $J = 2.0$ Hz, 1H), 7.57 (dd, $J = 15.2, 8.6$ Hz, 1H), 7.41 – 7.31 (m, 1H), 7.17 (td, $J = 8.5, 2.2$ Hz, 1H), 5.42 (s, 2H). ^{13}C NMR (150 MHz, DMSO- d_6) δ 171.2, 166.1, 161.5, 160.1, 148.7, 140.6, 140.4, 132.3, 125.6, 119.2, 113.3, 112.4, 104.6, 54.2. HRMS-ESI (–) m/z calculated for $\text{C}_{13}\text{H}_8\text{F}_2\text{NO}_4$ 280.0427 $[\text{M}-\text{H}]^-$, found: 280.0425.

1-(4-Chlorobenzyl)-5-hydroxy-4-oxo-1,4-dihydropyridine-3-carboxylic acid (10h). ^1H

NMR (600 MHz, DMSO- d_6): 10.08 (s, 1H), 8.69 (d, $J = 1.8$ Hz, 1H), 7.83 (d, $J = 1.8$ Hz, 1H), 7.48 (d, $J = 8.5$ Hz, 2H), 7.45 (d, $J = 8.5$ Hz, 2H), 5.34 (s, 2H). ^{13}C NMR (150 MHz, DMSO- d_6) δ 171.5, 166.5, 149.1, 140.6, 135.1, 133.8, 130.5, 129.4, 126.0, 113.7, 59.6. HRMS-ESI (–) m/z calculated for $\text{C}_{13}\text{H}_9\text{ClNO}_4$ 278.0226 $[\text{M}-\text{H}]^-$, found: 278.0222.

1-(3,4-Dichlorobenzyl)-5-hydroxy-4-oxo-1,4-dihydropyridine-3-carboxylic acid (10i).

^1H NMR (600 MHz, dmso): 10.08 (s, 1H), 8.72 (s, 1H), 7.87 (s, 1H), 7.81 (d, $J = 8.5$ Hz, 2H), 7.68 (s, 1H), 7.43 (d, $J = 8.5$ Hz, 2H), 5.33 (s, 2H). ^{13}C NMR (150 MHz, DMSO- d_6) δ 171.6, 166.5, 149.1, 140.9, 140.7, 137.0, 131.9, 131.6, 131.0, 128.9, 126.0, 113.8, 59.1. HRMS-ESI (–) m/z calculated for $\text{C}_{13}\text{H}_8\text{Cl}_2\text{NO}_4$ 311.9836 $[\text{M}-\text{H}]^-$, found: 311.9843.

1-(2,4-Dichlorobenzyl)-5-hydroxy-4-oxo-1,4-dihydropyridine-3-carboxylic acid (10j).

^1H NMR (600 MHz, DMSO- d_6): 10.12 (s, 1H), 8.58 (d, $J = 2.1$ Hz, 1H), 7.74 (d, $J = 2.2$ Hz, 1H), 7.50 (dd, $J = 8.3, 2.2$ Hz, 1H), 7.30 (d, $J = 8.3$ Hz, 1H), 5.47 (s, 2H). ^{13}C NMR

(150 MHz, DMSO-d₆) δ 171.7, 166.4, 149.0, 141.2, 134.7, 134.1, 132.7, 131.8, 129.8, 128.6, 126.2, 113.7, 57.8. HRMS-ESI (–) m/z calculated for C₁₃H₈Cl₂NO₄ 311.9836 [M-H][–], found: 311.9844.

1-(3-Chloro-4-fluorobenzyl)-5-hydroxy-4-oxo-1,4-dihydropyridine-3-carboxylic acid

(10k). ¹H NMR (600 MHz, DMSO-d₆): δ 10.07 (s, 1H), 8.72 (s, 1H), 7.87 (s, 1H), 7.80 (d, J = 6.5 Hz, 1H), 7.49–7.45 (m, 2H), 5.31 (s, 2H). ¹³C NMR (150 MHz, DMSO-d₆) δ 170.9, 165.9, 158.0, 148.5, 140.1, 133.3, 130.7, 129.2, 125.3, 119.8, 117.4, 113.2, 58.5. HRMS-ESI (–) m/z calculated for C₁₃H₈ClFNO₄ 296.0131 [M-H][–], found: 296.0134.

1-(4-Bromobenzyl)-5-hydroxy-4-oxo-1,4-dihydropyridine-3-carboxylic acid (10l).

¹H NMR (600 MHz, DMSO-d₆): δ 10.09 (s, 1H), 8.68 (d, J = 1.5 Hz, 1H), 7.83 (d, J = 1.5 Hz, 1H), 7.61 (d, J = 8.3 Hz, 2H), 7.38 (d, J = 8.3 Hz, 2H), 5.33 (s, 2H). ¹³C NMR (150 MHz, DMSO-d₆) δ 170.9, 165.9, 148.5, 140.9, 131.8, 130.2, 125.5, 121.9, 113.1, 59.1. HRMS-ESI (–) m/z calculated for C₁₃H₉BrNO₄ 321.9720 [M-H][–], found: 321.9727.

5-Hydroxy-4-oxo-1-(3-(trifluoromethyl)benzyl)-1,4-dihydropyridine-3-carboxylic acid (10m).

¹H NMR (600 MHz, DMSO-d₆): δ 10.09 (s, 1H), 8.75 (d, J = 2.1 Hz, 1H), 7.90–7.89 (m, 2H), 7.75 (d, J = 7.7 Hz, 1H), 7.72 (d, J = 7.8 Hz, 1H), 7.65 (t, J = 7.8 Hz, 1H), 5.43 (s, 2H). ¹³C NMR (150 MHz, DMSO-d₆) δ 171.0, 165.9, 148.5, 140.2, 136.8, 132.2, 130.0, 129.5, 125.4, 125.0, 124.9, 113.2, 59.1. HRMS-ESI (–) m/z calculated for C₁₄H₉F₃NO₄ 312.0489 [M-H][–], found: 312.0484.

5-Hydroxy-4-oxo-1-(pyridin-4-ylmethyl)-1,4-dihydropyridine-3-carboxylic acid (10n).

¹H NMR (600 MHz, CD₃OD): 8.74 (d, J = 4.9 Hz, 2H), 8.60 (d, J = 2.0 Hz, 1H), 7.69 (d, J = 2.0 Hz, 1H), 7.64 (d, J = 4.9 Hz, 2H), 5.57 (s, 2H). ¹³C NMR (150 MHz,

DMSO-d₆) δ HRMS-ESI (–) m/z calculated for C₁₂H₉N₂O₄ 245.0568 [M-H][–], found: 245.0570.

5-Hydroxy-1-(4-(methylsulfonyl)benzyl)-4-oxo-1,4-dihydropyridine-3-carboxylic

acid (10o). ¹H NMR (600 MHz, DMSO-d₆): δ 10.11 (s, 1H), 8.73 (d, J = 2.1 Hz, 1H), 7.96 (d, J = 8.3 Hz, 2H), 7.86 (d, J = 2.1 Hz, 1H), 7.64 (d, J = 8.3 Hz, 2H), 5.48 (s, 2H), 3.21 (s, 3H). ¹³C NMR (150 MHz, DMSO-d₆) δ 171.6, 166.5, 141.8, 141.3, 140.9, 129.2, 128.1, 126.1, 113.8, 87.2, 59.9, 44.4. HRMS-ESI (–) m/z calculated for C₁₄H₁₂NO₆S 322.0391 [M-H][–], found: 322.0382.

1-(4-Carboxybenzyl)-5-hydroxy-4-oxo-1,4-dihydropyridine-3-carboxylic acid (10p).

¹H NMR (600 MHz, DMSO-d₆): δ 13.04 (s, 1H), 10.09 (s, 1H), 8.69 (d, J = 2.0 Hz, 1H), 7.96 (d, J = 8.2 Hz, 2H), 7.83 (d, J = 2.1 Hz, 1H), 7.48 (d, J = 8.2 Hz, 2H), 5.44 (s, 2H). ¹³C NMR (150 MHz, DMSO-d₆) δ 171.2, 167.0, 166.2, 148.8, 140.5, 131.0, 130.1, 128.4, 128.0, 125.9, 113.4, 59.7. HRMS-ESI (–) m/z calculated for C₁₄H₁₀NO₆ 288.0514 [M-H][–], found: 288.0515.

5-Hydroxy-1-(4-methoxybenzyl)-4-oxo-1,4-dihydropyridine-3-carboxylic acid (10q).

¹H NMR (600 MHz, DMSO-d₆): δ 10.04 (s, 1H), 8.64 (d, J = 2.1 Hz, 1H), 7.82 (d, J = 2.1 Hz, 1H), 7.40 (d, J = 8.7 Hz, 2H), 6.96 (d, J = 8.7 Hz, 2H), 5.26 (s, 2H), 3.75 (s, 3H). ¹³C NMR (150 MHz, DMSO-d₆) δ 171.0, 166.3, 159.7, 148.6, 139.7, 130.0, 127.6, 125.7, 114.5, 113.3, 59.8, 55.4. HRMS-ESI (–) m/z calculated for C₁₄H₁₂NO₅ 274.0721 [M-H][–], found: 274.0722.

5-Hydroxy-1-(naphthalen-1-ylmethyl)-4-oxo-1,4-dihydropyridine-3-carboxylic acid

(10r). ¹H NMR (600 MHz, DMSO-d₆): δ 10.09 (s, 1H), 8.64 (d, J = 1.8 Hz, 1H), 8.07 (d, J = 8.3 Hz, 1H), 8.02 (d, J = 8.3 Hz, 1H), 8.00 (d, J = 8.4 Hz, 1H), 7.82 (d, J = 1.8 Hz, 1H),

7.64 (t, $J = 7.3$ Hz, 1H), 7.60 (t, $J = 7.3$ Hz, 1H), 7.56 (t, $J = 7.6$ Hz, 1H), 7.39 (d, $J = 7.6$ Hz, 1H), 5.90 (s, 2H). ^{13}C NMR (150 MHz, DMSO- d_6) δ 171.3, 166.4, 148.8, 140.4, 133.7, 131.2, 130.7, 129.7, 129.1, 127.4, 127.3, 126.7, 126.1, 126.0, 123.2, 113.5, 58.1. HRMS-ESI (–) m/z calculated for $\text{C}_{17}\text{H}_{12}\text{NO}_4$ 294.0772 $[\text{M-H}]^-$, found: 294.0776.

5-Hydroxy-1-(1-(naphthalen-1-yl)ethyl)-4-oxo-1,4-dihydropyridine-3-carboxylic acid

(10s). ^1H NMR (600 MHz, DMSO- d_6): δ 10.06 (s, 1H), 8.58 (d, $J = 1.8$ Hz, 1H), 8.05 (d, $J = 8.2$ Hz, 1H), 8.01 (dd, $J = 8.0, 4.0$ Hz, 2H), 7.86 (d, $J = 7.1$ Hz, 1H), 7.82 (d, $J = 1.8$ Hz, 1H), 7.66 (dd, $J = 16.0, 8.3$ Hz, 1H), 7.58 (dt, $J = 14.7, 6.9$ Hz, 2H), 6.59 (q, $J = 6.8$ Hz, 1H), 1.98 (d, $J = 6.8$ Hz, 3H). ^{13}C NMR (150 MHz, DMSO- d_6) δ 171.2, 166.4, 149.0, 138.4, 133.9, 133.0, 130.7, 130.4, 129.4, 127.6, 126.6, 126.1, 125.8, 124.3, 122.8, 113.6, 62.1, 20.7. HRMS-ESI (–) m/z calculated for $\text{C}_{18}\text{H}_{14}\text{NO}_4$ 308.0928 $[\text{M-H}]^-$, found: 308.0936.

5-Hydroxy-4-oxo-1-((1-phenylcyclopentyl)methyl)-1,4-dihydropyridine-3-carboxylic acid

(10t). ^1H NMR (600 MHz, DMSO- d_6): δ 9.82 (s, 2H), 7.70 (s, 2H), 7.29 (t, $J = 7.3$ Hz, 5H), 7.21 (dd, $J = 15.2, 7.4$ Hz, 7H), 7.09 (s, 2H), 4.32 (s, 5H), 1.94 (d, $J = 5.1$ Hz, 8H), 1.81 (s, 5H), 1.58 (s, 4H). HRMS-ESI (–) m/z calculated for $\text{C}_{18}\text{H}_{18}\text{NO}_4$ 312.1241 $[\text{M-H}]^-$, found: 312.1253.

1-([1,1'-Biphenyl]-2-ylmethyl)-5-hydroxy-4-oxo-1,4-dihydropyridine-3-carboxylic acid

(10u). ^1H NMR (600 MHz, DMSO- d_6): δ 9.94 (s, 1H), 8.04 (s, 1H), 7.50 – 7.44 (m, 2H), 7.44 – 7.39 (m, 2H), 7.38 (d, $J = 6.9$ Hz, 1H), 7.28 (dd, $J = 14.2, 7.0$ Hz, 5H), 5.36 (s, 2H). HRMS-ESI (–) m/z calculated for $\text{C}_{19}\text{H}_{14}\text{NO}_4$ 320.0928 $[\text{M-H}]^-$, found: 320.0936.

1-([1,1'-Biphenyl]-4-ylmethyl)-5-hydroxy-4-oxo-1,4-dihydropyridine-3-carboxylic acid

(10v). ^1H NMR (600 MHz, DMSO- d_6): δ 8.71 (s, 1H), 7.88 (s, 1H), 7.70 (d, $J = 7.7$

Hz, 2H), 7.66 (d, $J = 7.3$ Hz, 2H), 7.51 (d, $J = 7.6$ Hz, 2H), 7.46 (t, $J = 7.3$ Hz, 2H), 7.38 (d, $J = 7.2$ Hz, 1H), 5.40 (s, 2H). HRMS-ESI (–) m/z calculated for $C_{19}H_{14}NO_4$ 320.0928 [M-H][–], found: 320.0936.

1-((4'-(Aminomethyl)-[1,1'-biphenyl]-4-yl)methyl)-5-hydroxy-4-oxo-1,4-dihydropyridine-3-carboxylic acid (10w). ¹H NMR (600 MHz, DMSO-d₆): δ 10.10 (s, 1H), 8.71 (d, $J = 2.0$ Hz, 1H), 8.19 (s, 3H), 7.90 (d, $J = 2.0$ Hz, 1H), 7.74 (dd, $J = 8.2, 4.1$ Hz, 4H), 7.54 (dd, $J = 8.2, 5.3$ Hz, 4H), 5.40 (s, 2H), 4.08 (s, 2H). ¹³C NMR (150 MHz, DMSO-d₆) δ 171.6, 166.7, 149.2, 140.7, 140.3, 140.2, 135.7, 134.0, 130.1, 129.5, 127.9, 127.5, 126.4, 113.9, 60.3. HRMS-ESI (–) m/z calculated for $C_{20}H_{17}N_2O_4$ 349.1194 [M-H][–], found: 349.1196.

5-Hydroxy-4-oxo-1-(4-(quinolin-3-yl) benzyl)-1,4-dihydropyridine-3-carboxylic acid (10x). ¹H NMR (600 MHz, DMSO-d₆): δ 9.32 (d, $J = 2.1$ Hz, 1H), 8.80 (s, 1H), 8.74 (d, $J = 2.0$ Hz, 1H), 8.10 (t, $J = 7.9$ Hz, 2H), 7.96 (d, $J = 8.2$ Hz, 2H), 7.91 (d, $J = 2.0$ Hz, 1H), 7.84 (t, $J = 7.1$ Hz, 1H), 7.71 (t, $J = 7.4$ Hz, 1H), 7.63 (d, $J = 8.2$ Hz, 2H), 5.44 (s, 2H). ¹³C NMR (150 MHz, DMSO-d₆) δ 170.8, 166.0, 148.1, 148.0, 144.2, 139.9, 136.5, 135.7, 135.2, 132.2, 130.7, 128.9, 128.5, 127.7, 127.6, 126.5, 125.6, 113.1, 59.5. HRMS-ESI (–) m/z calculated for $C_{22}H_{15}N_2O_4$ 371.1037 [M-H], found: 371.1039.

5-Hydroxy-4-oxo-1-((4'-sulfamoyl-[1,1'-biphenyl]-4-yl)methyl)-1,4-dihydropyridine-3-carboxylic acid (10y). ¹H NMR (600 MHz, DMSO-d₆): δ 10.08 (s, 1H), 8.73 (d, $J = 2.0$ Hz, 1H), 7.89 (d, $J = 2.0$ Hz, 1H), 7.88 (d, $J = 8.6$ Hz, 2H), 7.86 (d, $J = 8.6$ Hz, 2H), 7.78 (d, $J = 8.2$ Hz, 2H), 7.55 (d, $J = 8.2$ Hz, 2H), 7.39 (s, 2H), 5.41 (s, 2H). ¹³C NMR (150 MHz, DMSO-d₆) δ 170.8, 165.9, 148.2, 142.9, 142.4, 139.9, 138.7, 135.5, 128.7, 127.0,

126.0, 125.5, 113.0, 59.4. HRMS-ESI (–) m/z calculated for $C_{19}H_{15}N_2O_6S$ 399.0656 [M–H], found: 399.0667.

5-Hydroxy-4-oxo-1-(4-(pyridin-3-yl) benzyl)-1,4-dihydropyridine-3-carboxylic acid

(10z). 1H NMR (600 MHz, DMSO- d_6): δ 9.01 (s, 1H), 8.73 (d, J = 1.9 Hz, 1H), 8.68 (d, J = 4.9 Hz, 1H), 8.33 (d, J = 7.9 Hz, 1H), 7.90 (d, J = 2.0 Hz, 1H), 7.82 (d, J = 8.2 Hz, 2H), 7.70 (dd, J = 7.8, 5.1 Hz, 1H), 7.59 (d, J = 8.1 Hz, 2H), 5.42 (s, 2H). ^{13}C NMR (150 MHz, DMSO- d_6) δ 171.1, 166.2, 148.7, 145.3, 144.4, 140.2, 138.3, 136.4, 136.3, 136.0, 129.1, 127.9, 125.8, 125.4, 113.4, 59.7. HRMS-ESI (–) m/z calculated for $C_{18}H_{13}N_2O_4$ 321.0881 [M–H], found: 321.0887.

Ethyl-1-(4-fluorobenzyl)-5-hydroxy-4-oxo-1,4-dihydropyridine-3-carboxylate (18).

1H NMR (600 MHz, CD_3OD): 8.50 (d, J = 1.2 Hz, 1H), 7.58 (d, J = 1.2 Hz, 1H), 7.41 (dd, J = 8.2, 5.4 Hz, 2H), 7.16 (t, J = 8.2 Hz, 2H), 5.25 (s, 2H), 4.34 (q, J = 7.1 Hz, 2H), 1.36 (t, J = 7.1 Hz, 3H). ^{13}C NMR (150 MHz, DMSO- d_6) δ 161.2, 156.1, 154.1, 142.5, 133.5, 123.4, 122.1, 113.2, 107.9, 105.7, 52.7, 52.1, 9.3. HRMS-ESI (–) m/z calculated for $C_{15}H_{13}FNO_4$ 290.0834 [M–H], found: 290.0837.

1-(4-Fluorobenzyl)-5-hydroxy-4-oxo-1,4-dihydropyridine-3-carboxamide (20).

1H NMR (600 MHz, DMSO- d_6): δ 9.44 (d, J = 4.2 Hz, 1H), 9.13 (s, 1H), 8.49 (d, J = 2.1 Hz, 1H), 7.65 (d, J = 2.1 Hz, 1H), 7.53 – 7.39 (m, 3H), 7.23 (t, J = 8.8 Hz, 2H), 5.23 (s, 2H). ^{13}C NMR (150 MHz, DMSO- d_6) δ 169.7, 165.6, 163.0, 161.4, 149.5, 139.9, 132.6, 130.5, 122.1, 116.0, 58.8. HRMS-ESI (–) m/z calculated for $C_{13}H_{10}FN_2O_3$ 261.0681 [M–H], found: 261.0681.

N-(2,4-difluorobenzyl)-1-(4-fluorobenzyl)-5-hydroxy-4-oxo-1,4-dihydropyridine-3-

carboxamide (22). 1H NMR (600 MHz, DMSO- d_6): δ 10.60 (t, J = 5.7 Hz, 1H), 9.20 (s,

1H), 8.51 (d, $J = 1.8$ Hz, 1H), 7.67 (d, $J = 1.8$ Hz, 1H), 7.46 (dd, $J = 8.2, 5.8$ Hz, 2H), 7.41 (dd, $J = 15.5, 8.4$ Hz, 1H), 7.23 (dd, $J = 14.5, 5.8$ Hz, 3H), 7.08 – 7.03 (m, 1H), 5.25 (s, 2H), 4.53 (d, $J = 5.7$ Hz, 2H). HRMS-ESI (–) m/z calculated for $C_{20}H_{14}N_2O_3$ 387.0962 [M–H], found: 387.0967.

Biology

Reagents

Biologicals. Recombinant HIV-1 reverse transcriptase (RT) was expressed and purified as previously described.³⁶ The catalytically active RNase H domain fragment of HIV-1 RT was expressed from plasmid pCSR231 (Dr. Daria Hazuda, Merck, West Point, PA) and purified as previously described.³⁷ P4R5 HIV infection indicator cells were obtained from the NIH AIDS Reagent Program, Division of AIDS, NIAID, NIH (p4R5.MAGI from Dr. Nathaniel Landau). These cells express CD4, CXCR4 and CCR5 as well as a β -galactosidase reporter gene under the control of an HIV LTR promoter.

Chemicals. DNA and RNA oligonucleotides for the preparation of RNA/DNA duplexes for assay of RNase H activity were purchased from Trilink (San Diego, CA).

RNase H assay. RNase H activity was measured essentially as previously described.²¹ Three different RNA/DNA duplex substrates were used, each assessing a different mode of RNase H cleavage. HTS-1 (RNA 5'-gaucugagccugggagcu-3'-fluorescein annealed to DNA 3'-CTAGACTCGGACCCTCGA-5'-Dabcyl) is a high sensitivity duplex that assesses non-specific internal cleavage. HTS-2 (RNA 5'-cugguuagaccagaucugagccugggagcu-3'-fluorescein annealed to DNA 3'-GGTCTAGACTCGGACCCTCGA-5'-Dabcyl) provides a duplex with a recessed DNA

3'-terminus and measures 3'-DNA directed or polymerase directed RNase H cleavage. HTS-3 (RNA 5'-accagaucugagccugggagcu-3-fluorescein annealed to DNA 3'-GACCAATCTGGTCTAGACTCGGACCCTCGA-5'-Dabcyl) measures 5'-RNA-directed RNase H cleavage.

RT polymerase assay. HIV RT polymerase activity was determined in the presence and the absence of inhibitor using 10 μ M [3 H]-TTP and 40nM poly(rA)-oligo(dT)16 (both obtained from Perkin Elmer, Waltham, MA) in 50 mM Tris-HCl, pH 7.4 (37°C) containing 60 mM KCl and 5 mM MgCl₂. Reactions were initiated by the addition of 10 nM WT or mutant RT and carried out for 20 min at 37°C. Reactions were quenched by 200 μ l ice cold 10% TCA containing 20 mM sodium pyrophosphate and filtered using a 1.2 μ m glass fiber filter 96-well plates (Millipore, Billerica, MA) followed by sequentially wash with 10% TCA and ethanol. The extent of radionucleotide incorporation was determined by liquid scintillation spectrometry.

Order-of-addition RNase H inhibition assays. Order-of-addition RNase H inhibition assays were carried out as previously described with some minor modifications.^{21, 38} Each reaction contained 100 nM HIV-1 RT, 6 mM MgCl₂, 250 nM RNA/DNA (HTS-1) substrate, 30 μ M inhibitor, and 1% DMSO. HIV-1 RT was pre-incubated with inhibitor, MgCl₂, and/or RNA/DNA (HTS-1) substrate in the following conditions at 37 °C for 10 min prior to starting the reaction: RT + inhibitor, RT + inhibitor + MgCl₂, RT + inhibitor + HTS-1, RT + HTS-1, and RT + HTS-1 + MgCl₂ + DMSO (no inhibitor control). The reactions were initiated by the addition of the missing components, and were run at 37 °C for 10 min. A control with only DMSO carrier was used to adjust the fluorescence signal

of the samples that contained inhibitor. Values are reported as mean \pm standard deviation from two independent experiments.

To mimic conditions similar to those in the virion, order-of-addition reactions containing 300 nM HIV-1 RT, 6 mM MgCl₂, 50 nM RNA/DNA (HTS-1) substrate, 0.5 mM EDTA, 30 μ M inhibitor, and 1% DMSO were also performed. HIV-1 RT was pre-incubated with inhibitor, MgCl₂, and/or RNA/DNA (HTS-1) substrate in the following conditions at 37 °C for 10 min prior to starting the reaction: RT + inhibitor, RT + HTS-1, and RT + HTS-1 + MgCl₂ + DMSO (no inhibitor control). The reactions were initiated by the addition of the missing components, and were run at 37 °C for 2 min. A control with only DMSO carrier was used to adjust the fluorescence signal of the samples that contained inhibitor. Values are reported as mean \pm standard deviation from two independent experiments.

HIV IN assay. HIV integrase was expressed and purified as previously reported.³⁹ Inhibition assays were performed using a modified protocol of our reported method.³⁹ Briefly, 2.1 μ L of compound suspended in DMSO was placed in duplicate into a Black 96 well non-binding plate (corning 3991). Compounds were plated in duplicate to a final concentration of 0.13 — 100 μ M. To each well of the plate 186.9 μ L of reaction mixture without DNA substrate was added (10 mM HEPES pH 7.5, 10 % glycerol w/v, 10 mM MnCl₂, 1 mM DTT, 1 μ M integrase). The enzyme was incubated with inhibitor for 10 min at 25 °C after which the reaction was initiated by the addition of 21 μ L of 500 nM oligo (5' biotin ATGTGGAAAATCTCTAGCA annealed with ACTGCTAGAGATTTTCCACAT 3' Cy5). Reactions were incubated at 37 °C for 30 min and then quenched by the addition of 5.2 μ L 500 mM EDTA. Each reaction was moved

(200 μ L) to a MultiScreen HTS PCR plate (Millipore MSSLBPC10) containing 20 μ L streptavidin agarose beads (Life Technologies S951) and incubated with shaking for 30 min. A vacuum manifold was used to remove the reaction mixture and the beads were similarly washed 3 times with wash buffer (.05% SDS, 1 mM EDTA in PBS). The plates were further washed 3 times with 200 μ L 50 mM NaOH to denature DNA not covalently linked to the biotin modification. For each denaturation step the plate was incubated with shaking at 25 °C for 5 min and the NaOH was removed by centrifugation at 1000 g for 1 min. The reaction products were eluted from the beads by the addition of 150 μ L formamide. The plate was incubated at 25 °C for 10 min and read directly at 635/675 in a SpectraMax i3 plate reader (Molecular Devices).

Antiviral assays. Antiviral assays were carried out using P4R5 indicator cells essentially as previously described.²³ P4R5 cells were cultured in 96-well microplates (5×10^3 cells per well) and maintained in DMEM/10% FBS supplemented with puromycin (0.5 μ g/ml). Cells were incubated in the presence or the absence of drug for 16h then exposed to HIV followed by an additional incubation period of 48h. The extent of infection was assessed using a fluorescence-based β -galactosidase detection assay, as previously described.⁴⁰

Modeling and docking analysis. Molecular modeling was performed using the Schrodinger small molecule drug discovery suite 2014-3. The crystal structure of HIV-1 RNase H p15 with engineered E.coli loop co-crystallized with pyrimidinol carboxylic acid (**5**) was extracted from the protein data bank (PDB code: 3HYF³¹) as reported by Lansdon et.al.¹⁴ The above structure was subjected to analysis and found that the native ligand, pyrimidinol carboxylic acid was bound to the active site of RNase H. This model was subjected to protein preparation wizard³²⁻³³ (Schrödinger Inc) in which missing hydrogens

atoms were added, zero-order bonds to metals were created followed by the generation of metal binding states. The structure of protein was minimized using OPLS 2005 force field³⁴ to optimize hydrogen bonding network and converge heavy atoms to the RMSD of 0.3 Å. The processed model indicates that the interaction between the pyrimidinol carboxylic acid (**5**) and RNase H is mediated by two metal cations (**Mn**²⁺) coordinated by the active site residues D443, E478, D498 and D549.

The receptor grid generation tool in Maestro (Schrodinger Inc) was used to define an active site around the native ligand (**5**) to cover all the residues within 12 Å from it with both the metal cofactors (**Mn**²⁺) as a constraint to identify the chelating triad during docking. Compounds **10r** and **10y** were drawn using Maestro and subjected to Lig Prep³⁵ to generate conformers, possible protonation at pH of 7±3 and metal binding states which serves as an input for docking process. All the dockings were performed using Glide XP²²⁻²³ (Glide, version 6.4) mode with both the **Mn**²⁺ metal cofactors as a constraint. The van der Waals radii of non-polar atoms for each of the ligands were scaled by a factor of 0.8. The predicted favorable binding mode of compounds **10r** and **10y** features the critical interaction between the chelating triad and to the divalent metal cofactors. All the ligands within the active site of RNase H were further refined post docking by minimizing under implicit solvent to account for the local protein flexibility.

HIV-1 RT crystallization and data collection. HIV-1 RT containing C280S mutations in the p66 and p51 subunits was expressed and purified as previously described.^{38, 41} Co-crystallization of HIV-1 RT with **10y** was achieved by mixing a solution of RT at a final concentration of 10 mg/ml, 50 mM MgCl₂, 5 mM tris(2-carboxyethyl)phosphine (TCEP) HCl, 0.5% β-octylglucoside, and 1 mM **10y** in a 1:1 ratio with a solution of 15% PEG 3500,

0.1 M sodium potassium phosphate, 5% ethylene glycol, and 0.1 M MES pH 6.1. Large, blocky crystals grew by hanging drop vapor diffusion at 18 °C in 2-3 days.

HIV-1 RT/**10y** co-crystals were additionally soaked with 1.5 mM **10y**, 5 mM TCEP HCl, 0.6% β -octylglucoside, 8% ethylene glycol, and 50 mM MgCl₂ for 20 minutes before brief cryoprotection in a solution containing 23% ethylene glycol and 4% trimethylamine N-oxide, followed by fast cryo-cooling in liquid nitrogen. Four data sets collected at Beamline 4.2.2 of the Advanced Light Source at Lawrence Berkeley National Laboratory were processed, scaled, and merged to 2.9 Å resolution using XDS.⁴² The HIV-1 RT/**10y** crystals were of space group P1, and had unit cell dimensions of $a = 69.1$ Å, $b = 89.3$ Å, $c = 108.2$ Å and $\alpha = 105.5^\circ$, $\beta = 92.7^\circ$, $\gamma = 110.8^\circ$. Two RT molecules were present in the asymmetric unit, and the Matthews coefficient was 2.5 Å³/Da, corresponding to a solvent content of 51.6%.⁴³ Crystal data and statistics are listed in SI Table 1.

Phase determination and structure refinement. The structure was determined by molecular replacement using Phaser.⁴⁴ A crystal structure of unliganded HIV-1 RT (Protein Data Bank code 1DLO) was used as an initial search model for a related higher resolution structure (2.28 Å) of an unpublished P1 RT/RNase H inhibitor complex with two molecules in the asymmetric unit. Rigid-body, simulated annealing (to remove bias), atomic displacement parameter (ADP), real-space and restrained refinement were performed on this initial model using Phenix.⁴⁵ Several cycles of model building and refinement were carried out using Coot⁴⁶ and Phenix or Refmac,⁴⁷ respectively, for the related higher resolution RT/RNase H inhibitor complex, and this final model was used as the search model for molecular replacement of the RT/**10y** complex using the above

1
2
3 protocols. The final RT/**10y** structure was validated using MolProbity.⁴⁸ Final refinement
4
5 statistics are listed in SI Table 1.
6
7

8 9 **ASSOCIATED CONTENT**

10
11
12 **Supporting Information Available.** Chemical synthesis, general procedures, spectral
13 data, including ¹H NMR of intermediates (**16a-16s**; **17a-17s**, **17w-17z**), and
14
15 crystallographic data and refinement statistics are available in the supporting information.
16
17 This material is available free of charge via the Internet at <http://pubs.acs.org>.
18
19

20
21
22 **PDB ID.** The atomic coordinates and structure factors have been deposited in the RCSB
23 Protein Data Bank (PDB ID: 5J1E). Authors will release the atomic coordinates and
24
25 experimental data upon article publication.
26
27
28
29

30 31 **AUTHOR INFORMATION**

32 33 **Corresponding Author**

34
35 Email: wangx472@umn.edu; Phone: +1 (612) 626-7025.
36
37
38
39

40 41 **ACKNOWLEDGMENTS**

42
43 This research was supported in part by the National Institutes of Health (AI100890 to SGS,
44 MAP and ZW), and by the Research Development and Seed Grant Program of the Center
45 for Drug Design, University of Minnesota. The Advanced Light Source is supported by
46
47 the Director, Office of Science, Office of Basic Energy Sciences, of the U.S. Department
48
49 of Energy under Contract No. DE-AC02-05CH11231.
50
51
52
53
54

55 56 **ABBREVIATIONS USED**

57
58
59
60

RT, reverse transcriptase; RNase H or RNH, ribonuclease H; HIV, human immunodeficiency virus; IN, integrase; NRTIs, nucleoside RT inhibitors; NNRTIs, nonnucleoside RT inhibitors; INST, integrase strand transfer; SAR, structure-activity-relationship; MW, Microwave;

Reference

1. <http://www.unaids.org/en/dataanalysis/datatools/aidsinfo/>.
2. Yeni, P., Update on HAART in HIV. *J. Hepatol.* **2006**, *44*, S100-103.
3. Tramontano, E.; Di Santo, R., HIV-1 RT-associated RNase H function inhibitors: recent advances in drug development. *Curr. Med. Chem.* **2010**, *17*, 2837-2853.
4. Sarafianos, S. G.; Marchand, B.; Das, K.; Himmel, D. M.; Parniak, M. A.; Hughes, S. H.; Arnold, E., Structure and function of HIV-1 reverse transcriptase: molecular mechanisms of polymerization and inhibition. *J. Mol. Biol.* **2009**, *385*, 693-713.
5. Cihlar, T.; Ray, A. S., Nucleoside and nucleotide HIV reverse transcriptase inhibitors: 25 years after zidovudine. *Antiviral Res.* **2010**, *85*, 39-58.
6. de Bethune, M. P., Non-nucleoside reverse transcriptase inhibitors (NNRTIs), their discovery, development, and use in the treatment of HIV-1 infection: a review of the last 20 years (1989-2009). *Antiviral Res.* **2010**, *85*, 75-90.
7. HIV drugs in development. <http://www.thebody.com/index/treat/newdrugs.html> (accessed 2016).
8. Parniak, M. A. Unpublished data
9. Cao, L.; Song, W.; De Clercq, E.; Zhan, P.; Liu, X., Recent progress in the research of small molecule HIV-1 RNase H inhibitors. *Curr. Med. Chem.* **2014**, *21*, 1956-1967.

- 1
2
3
4
5
6
7
8
9
10
11
12
13
14
15
16
17
18
19
20
21
22
23
24
25
26
27
28
29
30
31
32
33
34
35
36
37
38
39
40
41
42
43
44
45
46
47
48
49
50
51
52
53
54
55
56
57
58
59
60
10. Klumpp, K.; Hang, J. Q.; Rajendran, S.; Yang, Y. L.; Derosier, A.; In, P. W. K.; Overton, H.; Parkes, K. E. B.; Cammack, N.; Martin, J. A., Two-metal ion mechanism of RNA cleavage by HIV RNase H and mechanism-based design of selective HIV RNase H inhibitors. *Nucleic Acids Res.* **2003**, *31*, 6852-6859.
11. Himmel, D. M.; Maegley, K. A.; Pauly, T. A.; Bauman, J. D.; Das, K.; Dharia, C.; Clark, A. D., Jr.; Ryan, K.; Hickey, M. J.; Love, R. A.; Hughes, S. H.; Bergqvist, S.; Arnold, E., Structure of HIV-1 reverse transcriptase with the inhibitor beta-Thujaplicinol bound at the RNase H active site. *Structure* **2009**, *17*, 1625-1635.
12. Himmel, D. M.; Myshakina, N. S.; Ilina, T.; Van Ry, A.; Ho, W. C.; Parniak, M. A.; Arnold, E., Structure of a dihydroxycoumarin active-site inhibitor in complex with the RNase H domain of HIV-1 reverse transcriptase and structure-activity analysis of inhibitor analogs. *J. Mol. Biol.* **2014**, *426*, 2617-2631.
13. Shaw-Reid, C. A.; Munshi, V.; Graham, P.; Wolfe, A.; Witmer, M.; Danzeisen, R.; Olsen, D. B.; Carroll, S. S.; Embrey, M.; Wai, J. S.; Miller, M. D.; Cole, J. L.; Hazuda, D. J., Inhibition of HIV-1 ribonuclease H by a novel diketo acid, 4-[5-(benzoylamino)thien-2-yl]-2,4-dioxobutanoic acid. *J. Biol. Chem.* **2003**, *278*, 2777-2780.
14. Kirschberg, T. A.; Balakrishnan, M.; Squires, N. H.; Barnes, T.; Brendza, K. M.; Chen, X.; Eisenberg, E. J.; Jin, W.; Kutty, N.; Leavitt, S.; Liclican, A.; Liu, Q.; Liu, X.; Mak, J.; Perry, J. K.; Wang, M.; Watkins, W. J.; Lansdon, E. B., RNase H active site inhibitors of human immunodeficiency virus type 1 reverse transcriptase: design, biochemical activity, and structural information. *J. Med. Chem.* **2009**, *52*, 5781-5784.

- 1
2
3
4
5
6
7
8
9
10
11
12
13
14
15
16
17
18
19
20
21
22
23
24
25
26
27
28
29
30
31
32
33
34
35
36
37
38
39
40
41
42
43
44
45
46
47
48
49
50
51
52
53
54
55
56
57
58
59
60
15. Williams, P. D.; Staas, D. D.; Venkatraman, S.; Loughran, H. M.; Ruzek, R. D.; Booth, T. M.; Lyle, T. A.; Wai, J. S.; Vacca, J. P.; Feuston, B. P.; Ecto, L. T.; Flynn, J. A.; DiStefano, D. J.; Hazuda, D. J.; Bahnck, C. M.; Himmelberger, A. L.; Dornadula, G.; Hrin, R. C.; Stillmock, K. A.; Witmer, M. V.; Miller, M. D.; Grobler, J. A., Potent and selective HIV-1 ribonuclease H inhibitors based on a 1-hydroxy-1,8-naphthyridin-2(1H)-one scaffold. *Bioorg. Med. Chem. Lett.* **2010**, *20*, 6754-6757.
16. Beilhartz, G. L.; Ngure, M.; Johns, B. A.; Deanda, F.; Gerondelis, P.; Gotte, M., Inhibition of the ribonuclease H activity of HIV-1 reverse transcriptase by GSK5750 correlates with slow enzyme-inhibitor dissociation. *J. Biol. Chem.* **2014**, *289*, 16270-16277.
17. Nowotny, M., Retroviral integrase superfamily: the structural perspective. *EMBO Rep.* **2009**, *10*, 144-151.
18. Fujishita, T.; Mikamiyama, M.; Kawai, M.; Akiyama, T. Substituted 3-hydroxy-4-pyridone derivative. WO2010110231, 2010.
19. Johns, B. A.; Kawasuji, T.; Weatherhead, J. G.; Taishi, T.; Temelkoff, D. P.; Yoshida, H.; Akiyama, T.; Taoda, Y.; Murai, H.; Kiyama, R.; Fuji, M.; Tanimoto, N.; Jeffrey, J.; Foster, S. A.; Yoshinaga, T.; Seki, T.; Kobayashi, M.; Sato, A.; Johnson, M. N.; Garvey, E. P.; Fujiwara, T., Carbamoyl pyridone HIV-1 integrase inhibitors 3. A diastereomeric approach to chiral nonracemic tricyclic ring systems and the discovery of dolutegravir (S/GSK1349572) and (S/GSK1265744). *J. Med. Chem.* **2013**, *56*, 5901-5916.
20. Vernekar, S. K. V.; Liu, Z.; Nagy, E.; Miller, L.; Kirby, K. A.; Wilson, D. J.; Kankanala, J.; Sarafianos, S. G.; Parniak, M. A.; Wang, Z. Q., Design, synthesis,

biochemical, and antiviral evaluations of C6 benzyl and C6 biarylmethyl substituted 2-hydroxyisoquinoline-1,3-diones: dual inhibition against HIV reverse transcriptase-associated RNase H and polymerase with antiviral activities. *J. Med. Chem.* **2015**, *58*, 651-664.

21. Parniak, M. A.; Min, K. L.; Budihias, S. R.; Le Grice, S. F.; Beutler, J. A., A fluorescence-based high-throughput screening assay for inhibitors of human immunodeficiency virus-1 reverse transcriptase-associated ribonuclease H activity. *Anal. Biochem.* **2003**, *322*, 33-39.
22. Beilhartz, G. L.; Wendeler, M.; Baichoo, N.; Rausch, J.; Le Grice, S.; Gotte, M., HIV-1 reverse transcriptase can simultaneously engage its DNA/RNA substrate at both DNA polymerase and RNase H active sites: implications for RNase H inhibition. *J. Mol. Biol.* **2009**, *388*, 462-474.
23. Sirivolu, V. R.; Vernekar, S. K. V.; Ilina, T.; Myshakina, N. S.; Parniak, M. A.; Wang, Z. Q., Clicking 3'-azidothymidine into novel potent inhibitors of human immunodeficiency virus. *J. Med. Chem.* **2013**, *56*, 8765-8780.
24. ***Small-molecule drug discovery suite 2014-3: Glide, version 6.4, Schrödinger, LLC, New York: 2014.***
25. Friesner, R. A.; Murphy, R. B.; Repasky, M. P.; Frye, L. L.; Greenwood, J. R.; Halgren, T. A.; Sanschagrin, P. C.; Mainz, D. T., Extra precision glide: docking and scoring incorporating a model of hydrophobic enclosure for protein-ligand complexes. *J. Med. Chem.* **2006**, *49*, 6177-6196.

26. Huang, H.; Chopra, R.; Verdine, G. L.; Harrison, S. C., Structure of a covalently trapped catalytic complex of HIV-1 reverse transcriptase: implications for drug resistance. *Science* **1998**, *282*, 1669-1675.
27. Sarafianos, S. G.; Das, K.; Tantillo, C.; Clark, A. D., Jr.; Ding, J.; Whitcomb, J. M.; Boyer, P. L.; Hughes, S. H.; Arnold, E., Crystal structure of HIV-1 reverse transcriptase in complex with a polypurine tract RNA:DNA. *EMBO J.* **2001**, *20*, 1449-1461.
28. Su, H.-P.; Yan, Y.; Prasad, G. S.; Smith, R. F.; Daniels, C. L.; Abeywickrema, P. D.; Reid, J. C.; Loughran, H. M.; Kornienko, M.; Sharma, S.; Grobler, J. A.; Xu, B.; Sardana, V.; Allison, T. J.; Williams, P. D.; Darke, P. L.; Hazuda, D. J.; Munshi, S., Structural Basis for the Inhibition of RNase H activity of HIV-1 reverse transcriptase by RNase H active site-directed inhibitors. *J. Virol.* **2010**, *84*, 7625-7633.
29. Lansdon, E. B.; Liu, Q.; Leavitt, S. A.; Balakrishnan, M.; Perry, J. K.; Lancaster-Moyer, C.; Kutty, N.; Liu, X.; Squires, N. H.; Watkins, W. J.; Kirschberg, T. A., Structural and binding analysis of pyrimidinol carboxylic acid and N-hydroxy quinazolinedione HIV-1 RNase H inhibitors. *Antimicrob. Agents Chemother.* **2011**, *55*, 2905-2915.
30. Rodgers, D. W.; Gamblin, S. J.; Harris, B. A.; Ray, S.; Culp, J. S.; Hellmig, B.; Woolf, D. J.; Debouck, C.; Harrison, S. C., The structure of unliganded reverse-transcriptase from the human-immunodeficiency-virus Type-1. *Proc. Natl. Acad. Sci. USA* **1995**, *92*, 1222-1226.
31. Hsiou, Y.; Ding, J.; Das, K.; Clark, A. D.; Hughes, S. H.; Arnold, E., Structure of unliganded HIV-1 reverse transcriptase at 2.7 angstrom resolution: implications of

- conformational changes for polymerization and inhibition mechanisms. *Structure* **1996**, *4*, 853-860.
32. Sarafianos, S. G.; Das, K.; Clark, A. D., Jr.; Ding, J.; Boyer, P. L.; Hughes, S. H.; Arnold, E., Lamivudine (3TC) resistance in HIV-1 reverse transcriptase involves steric hindrance with beta-branched amino acids. *Proc. Natl. Acad. Sci. USA* **1999**, *96*, 10027-10032.
33. Hsiou, Y.; Ding, J. P.; Das, K.; Clark, A. D.; Boyer, P. L.; Lewi, P.; Janssen, P. A. J.; Kleim, J. P.; Rosner, M.; Hughes, S. H.; Arnold, E., The Lys103Asn mutation of HIV-1 RT: a novel mechanism of drug resistance. *J. Mol. Biol.* **2001**, *309*, 437-445.
34. Tu, X. Y.; Das, K.; Han, Q. W.; Bauman, J. D.; Clark, A. D.; Hou, X. R.; Frenkel, Y. V.; Gaffney, B. L.; Jones, R. A.; Boyer, P. L.; Hughes, S. H.; Sarafianos, S. G.; Arnold, E., Structural basis of HIV-1 resistance to AZT by excision. *Nat. Struct. Mol. Biol.* **2010**, *17*, 1202-1209.
35. PyMOL: www.pymol.org (accessed 2016).
36. Fletcher, R. S.; Holleschak, G.; Nagy, E.; Arion, D.; Borkow, G.; Gu, Z.; Wainberg, M. A.; Parniak, M. A., Single-step purification of recombinant wild-type and mutant HIV-1 reverse transcriptase. *Protein Expres. Purif.* **1996**, *7*, 27-32.
37. Gong, Q.; Menon, L.; Ilina, T.; Miller, L. G.; Ahn, J.; Parniak, M. A.; Ishima, R., Interaction of HIV-1 reverse transcriptase ribonuclease H with an acylhydrazone inhibitor. *Chem. Biol. Drug Des.* **2011**, *77*, 39-47.
38. Kirby, K. A.; Marchand, B.; Ong, Y. T.; Ndongwe, T. P.; Hachiya, A.; Michailidis, E.; Leslie, M. D.; Sietsema, D. V.; Fetterly, T. L.; Dorst, C. A.; Singh, K.; Wang, Z.; Parniak, M. A.; Sarafianos, S. G., Structural and inhibition studies of the RNase H

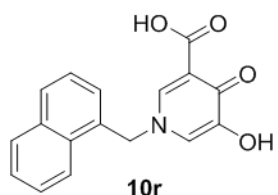
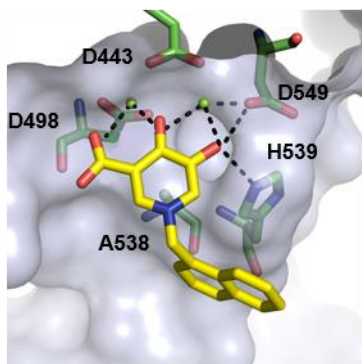
- function of xenotropic murine leukemia virus-related virus reverse transcriptase. *Antimicrob. Agents Chemother.* **2012**, *56*, 2048-2061.
39. Wang, Z.; Bennett, E. M.; Wilson, D. J.; Salomon, C.; Vince, R., Rationally designed dual inhibitors of HIV reverse transcriptase and integrase. *J. Med. Chem.* **2007**, *50*, 3416-3419.
40. Abram, M. E.; Parniak, M. A., Virion instability of human immunodeficiency virus type 1 reverse transcriptase (RT) mutated in the protease cleavage site between RT p51 and the RT RNase H domain. *J. Virol.* **2005**, *79*, 11952-11961.
41. Bauman, J. D.; Das, K.; Ho, W. C.; Baweja, M.; Himmel, D. M.; Clark, A. D.; Oren, D. A.; Boyer, P. L.; Hughes, S. H.; Shatkin, A. J.; Arnold, E., Crystal engineering of HIV-1 reverse transcriptase for structure-based drug design. *Nucleic Acids Res.* **2008**, *36*, 5083-5092.
42. Kabsch, W., XDS. *Acta Crystallogr. D Biol. Crystallogr.* **2010**, *66*, 125-132.
43. Matthews, B. W., Determination of Protein Molecular-weight, hydration, and packing from crystal density. *Method Enzymol.* **1985**, *114*, 176-187.
44. McCoy, A. J.; Grosse-Kunstleve, R. W.; Adams, P. D.; Winn, M. D.; Storoni, L. C.; Read, R. J., Phaser crystallographic software. *J. Appl. Crystallogr.* **2007**, *40*, 658-674.
45. Adams, P. D.; Grosse-Kunstleve, R. W.; Hung, L. W.; Ioerger, T. R.; McCoy, A. J.; Moriarty, N. W.; Read, R. J.; Sacchettini, J. C.; Sauter, N. K.; Terwilliger, T. C., PHENIX: building new software for automated crystallographic structure determination. *Acta Crystallogr. D Biol. Crystallogr.* **2002**, *58*, 1948-1954.
46. Emsley, P.; Cowtan, K., Coot: model-building tools for molecular graphics. *Acta Crystallogr. D Biol. Crystallogr.* **2004**, *60*, 2126-2132.

1
2
3
4
5
6
7
8
9
10
11
12
13
14
15
16
17
18
19
20
21
22
23
24
25
26
27
28
29
30
31
32
33
34
35
36
37
38
39
40
41
42
43
44
45
46
47
48
49
50
51
52
53
54
55
56
57
58
59
60

47. Murshudov, G. N.; Vagin, A. A.; Dodson, E. J., Refinement of macromolecular structures by the maximum-likelihood method. *Acta Crystallogr. D Biol. Crystallogr.* **1997**, *53*, 240-255.

48. Davis, I. W.; Leaver-Fay, A.; Chen, V. B.; Block, J. N.; Kapral, G. J.; Wang, X.; Murray, L. W.; Arendall, W. B.; Snoeyink, J.; Richardson, J. S.; Richardson, D. C., MolProbity: all-atom contacts and structure validation for proteins and nucleic acids. *Nucleic Acids Res*, **2007**, *35*, W375-W383.

TOC Graphics



IC_{50} (RNase H) = 2.7 μ M

IC_{50} (RT pol) = 8.5 μ M

IC_{50} (IN) = 23 μ M

EC_{50} (HIV-1) = 10 μ M

CC_{50} > 25 μ M